J. Fluid Mech. (1991), *vol.* 223, *pp.* 253–311
Printed in Great Britain

Mode selection and resonant phase locking in unstable axisymmetric jets

By T. C. CORKE, F. SHAKIB AND H. M. NAGIB

Fluid Dynamics Center, Mechanical and Aerospace Engineering Department, Illinois Institute of Technology, Chicago, IL 60616, USA

(Received 23 June 1989 and in revised form 6 July 1990)

This paper presents experimental results on the nonlinear phase locking present in the resonant growth of unstable modes in the shear layer of an axisymmetric jet. The initial instability modes scale with the exiting shear layer and grow convectively with downstream distance. Because of the special condition at the exit lip of the jet, the initial growth of modes is very sensitive to local unsteady pressure fields. A part of the unsteady field is stochastic in nature. To a larger extent, the pressure field at the lip of the jet contains the imprint of the downstream-developing instability modes, in particular the first unstable axisymmetric mode and its subharmonic. These are felt at the lip of the jet as a result of the energetic processes of the first vortex rollup and vortex pairing. As a result, a resonant feedback exists which under special conditions makes the initial region of this flow in some sense absolutely unstable. The features of this process are brought out by the normalized cross-bispectrum or cross-bicoherence between the instantaneous unsteady pressure at the lip of the jet and velocity time series measured at the same azimuthal position for different downstream locations. These give a measure of the nonlinear phase locking between the principle modes and their sum and difference modes. Analysis of these show a perfect nonlinear phase locking at the fundamental axisymmetric and subharmonic frequencies between the pressure field at the lip and the velocity field at the downstream locations corresponding to the energy saturations of the fundamental and subharmonic modes. This resonance process can be suppressed or enhanced by low-amplitude axisymmetric mode forcing at the natural preferred frequency of slightly detuned cases. Contrasted to this is the behaviour of the fundamental $m = \pm 1$ helical mode. This mode was found to have the same spatial growth rate as the axisymmetric mode and a streamwise frequency approximately 20% higher, in agreement with theoretical predictions. However, short-time spectral estimates showed that these two fundamental modes do not exist at the same time or space. This suggests that each is a basin of attraction which suppresses the existence of the other. The apparent non-deterministic switching observed between these modes is probably the result of the response of the jet to stochastic input of axisymmetric or non-axisymmetric disturbances. This scenario may lead to a low-dimensional temporal model based on the interaction between these two modes which captures most of the early random nature seen in our experiments.

1. Axisymmetric jet

1.1 *Introduction*

For many years investigations have been conducted to understand the flow processes that occur in jets. One practical purpose of these was to determine the relationship

between the observed characteristic velocity fluctuations in the jet and the generation of measured far-field acoustic disturbances associated with these flows. Previous investigations in naturally and artificially excited jets have determined the importance of two instability lengthscales: one associated with the initial shear-layer thickness at the exit of the nozzle, and the other associated with the jet diameter which governs the shape of the mean velocity profile at the end of the potential core. The instability modes in the first region develop through continuous and gradual frequency and phase adjustments to produce a smooth merging with the second region. This process makes this problem fundamentally interesting, and for that reason it has received a great deal of attention. An excellent review of free-shear flows of the type discussed here is given by Ho & Huerre (1984). As a result, only a short review of past related work is presented here in order to help to focus on the singular characteristic of resonant axisymmetric mode phase locking that can exist in these flows.

1.2. *Background*

The shear-layer development just past the exit edge of a jet is initially dominated by a linear instability mechanism. The vorticity distribution is inviscidly unstable to small perturbations through a Kelvin–Helmholtz instability mechanism. These instability waves grow exponentially with streamwise distance, and when finite amplitudes are reached, roll up into discreet vortices.

In experiments in low-disturbance axisymmetric jet flows, most emphasis has been placed on the growth of axisymmetric disturbances close to the nozzle exit. The analysis of Michalke (1971), however, pointed out that the first helical mode has amplification characteristics in this region which are nearly identical to those of the fundamental axisymmetric mode. His analysis further suggests that as the shear layer thickens or grows, the amplification of the helical mode becomes more dominant over the axisymmetric mode. Mattingly & Chang (1974) performed a similar analysis with a different prescribed mean velocity distribution that showed that the amplification of the axisymmetric mode was only approximately 12% larger than that for the helical mode, and that the streamwise frequency of the most amplified helical disturbance in that case was approximately 20% higher than that of the most amplified axisymmetric mode. Drubka (1981) experimentally verified these results from cross-spectral and azimuthal phase measurements between velocity fluctuations in the shear layer and pressure fluctuations at the lip of a very low-disturbance axisymmetric jet flow.

The fact that the growth of the subharmonic of the initial axisymmetric mode leads to the downstream pairing of neighbouring vortices is now well established. In a two-dimensional mixing layer, Winant & Browand (1974) concluded that the successive pairing of neighbouring vortices was a primary mechanism for the streamwise growth of the shear layer. In a more recent experiment, Ho & Huang (1982) documented, for a harmonically forced mixing layer, that the first few pairings were accompanied by an approximate doubling of the shear-layer momentum thickness. This observation points to the potential importance of this fundamental process in jet mixing and spreading.

Focusing on the growth of subharmonic disturbances, Kelly (1967), in a linear temporal formulation, determined that when the amplitude of a fundamental instability wave reaches a finite value in the presence of a subharmonic wave, another instability mechanism based on a subharmonic resonance can arise. This mechanism requires that both waves have the same phase speed. This subharmonic resonance is weakly nonlinear and described by the Mathieu equation.

As the initially linear instability grows in amplitude toward a finite value, the shear layer begins to roll up to form discrete vortices. At this point the problem is fully nonlinear and is therefore past the range of validity of the linear model, such as for Kelly (1967). Pierrhumbert (1980) examined the effect of this nonlinearity on the subharmonic resonance. His results predicted that the nonlinearity associated with the rolled-up vortices enhances the growth of the subharmonic instability. The growth of the subharmonic mode is important in the sense of describing the mechanism for the pairing of ring vortices observed in an early experiment by Wille (1963).

Browand & Laufer (1975), Bruun (1977), Peterson (1978), Hussain & Clark (1981) and Laufer & Zhang (1983), among others, documented the effect of pairing on the growth of axisymmetric jets. Acton (1980) modelled discrete vortex ring elements and computationally followed the development of the instability wave into eddies, with and without forcing. Reasonable agreement was observed between this axisymmetric model and the experiments, thereby drawing the speculation that the large-scale structures in the jet are essentially axisymmetric. Ho (1981) based his subharmonic evolution model on this assumption.

External harmonic forcing of the jet has been used by many investigators to organize the streamwise location where the shear layer first rolls up as well as the pairing location. This forcing has invariably been large amplitude and axisymmetric. Kibens (1979) showed that when the initial instability frequency is related to the final 'preferred' jet instability frequency by an integer power of two, the jet becomes organized, vortex pairings are localized and the development of the initial shear-layer frequency towards the final preferred jet frequency occurs through an integer number of pairings. Although this was first observed in an externally excited jet, Drubka (1981) documented the same phenomenon for his 'low'-disturbance unexcited condition at a Reynolds number of 42000. At this condition, Drubka (1981) also noted the largest pressure fluctuations at the lip at a frequency corresponding to the subharmonic of the axisymmetric mode. From these results, he suggested a natural self-excitation for this organized pairing state.

Although the exact mechanism of pairing is not completely understood, a number of physical observations associated with this process have been made. When the initial axisymmetric subharmonic mode grows to a certain high amplitude, a secondary instability, the subharmonic resonance, develops. Petersen (1978) and Drubka (1981) reported that during resonance the subharmonic wave attains the same phase speed as the fundamental wave. This occurs after approximately two fundamental wavelengths. Beyond this point, the amplitude of the subharmonic mode increases to grow beyond that of the fundamental and vortex pairing is observed to occur. This point of pairing closely corresponds to the amplitude maximum of the subharmonic mode as shown by Ho & Huang (1982).

The vortex rollup and pairing are not generally expected to occur at a fixed streamwise location. Owing to the doubling in momentum thickness measured by Ho & Huang (1982) at pairing, such behaviour would result in a stepwise growth of the shear layer. However, Laufer & Zhang (1983) explained that in general the location of the pairing moves randomly in time and space, which results on the average in a smooth spreading rate.

Sarohia & Massier (1978) showed that a significant part of the pressure signal in the near field of a jet was generated by the pairing interaction and merging process. Laufer & Zhang (1983) suggest that the induced perturbations at the nozzle exit are the volume integral effect of all the fluctuations existing in the flow, with the largest

contribution coming from the subharmonic fluctuation at the pairing location. These pressure fluctuations induced by the unsteady flow downstream can set up an unsteady Kutta condition at the sharp trailing lip of the jet. This phenomenon and the fact that acoustic forcing further organizes the jet suggest that the fluctuations caused by the merging vortices propagate upstream and create a strong feedback-loop mechanism in the jet. Ho & Huang (1982) state that the location of the vortex merging can be predicted from the feedback loop evolution. This prediction is made by requiring the number of waves in the feedback loop to be an exact integer.

The organization of the jet flow and feedback accompanying pairing makes it a likely mechanism for acoustic wave generation. Ffowcs Williams & Kempton (1978) from their numerical calculations suggested that the pairing of eddies is the primary mechanism for the production of noise. Since the location of pairing can vary over a distance comparable with one eddy separation distance, the radiated sound is broadband. Sarohia & Massier (1978) add that the merging process has a statistical distribution of length and life span, so that it is quite probable that the emitted jet noise can appear to be broadband. Kibens (1979) observed, however, that in a forced jet, the resulting increase in noise consisted of tones at the subharmonics of the excitation frequency, which was accompanied by a reduction of the broadband noise.

1.3. *Objectives*

The object of this study was to further document the relation between the axisymmetric fundamental and subharmonic modes by following their development and interaction in the velocity field from the lip of the jet to beyond the point of vortex pairing. We hoped to identify the role of the feedback in this process and to locate the region of the maximum shear-layer influence. Furthermore, we intended to document the interactions between these and other instability modes, including non-axisymmetric (helical) modes leading to the appearance of other multiple-interaction modes. Such information, we felt, would be necessary to point to efficient and predictable means of controlling these jet flows.

Two Reynolds numbers were examined, one being Drubka's $Re = 42000$ case at which a natural coupling existed between the initial and final jet instability frequencies and, as a contrast, one at which no special coupling existed. The effect of initial conditions on these jets was examined by increasing the broad-spectrum turbulence intensity within the jet core and by very low-amplitude narrowband external acoustic forcing. The forcing was intended to favour axisymmetric modes. A level of the forcing was chosen to be comparable with the levels in the natural feedback so as to mutually enhance or compete with that mechanism.

2. Experimental set-up

As in the case of Drubka (1981), this study was conducted in the IIT Jet Facility. A detailed description of that facility and the characteristics of the jet flow are contained in that reference and will not be presented here. Benchmarking measurements, documented in the thesis by Shakib (1984), were taken to confirm that the flow conditions were the same as for that previous work.

Two of Drubka's flow cases were used in this study. The first was his lowest initial disturbance condition ($u'/U_j = 0.05\%$) designated 1L, and the other his highest initial disturbance jet condition ($u'/U_j = 0.16\%$) designated 3L. A scale drawing of the exit face of the nozzel is shown at the top of figure 1. The exit diameter of the jet in this figure is 5.14 cm. As shown in this drawing, eight azimuthal pressure taps

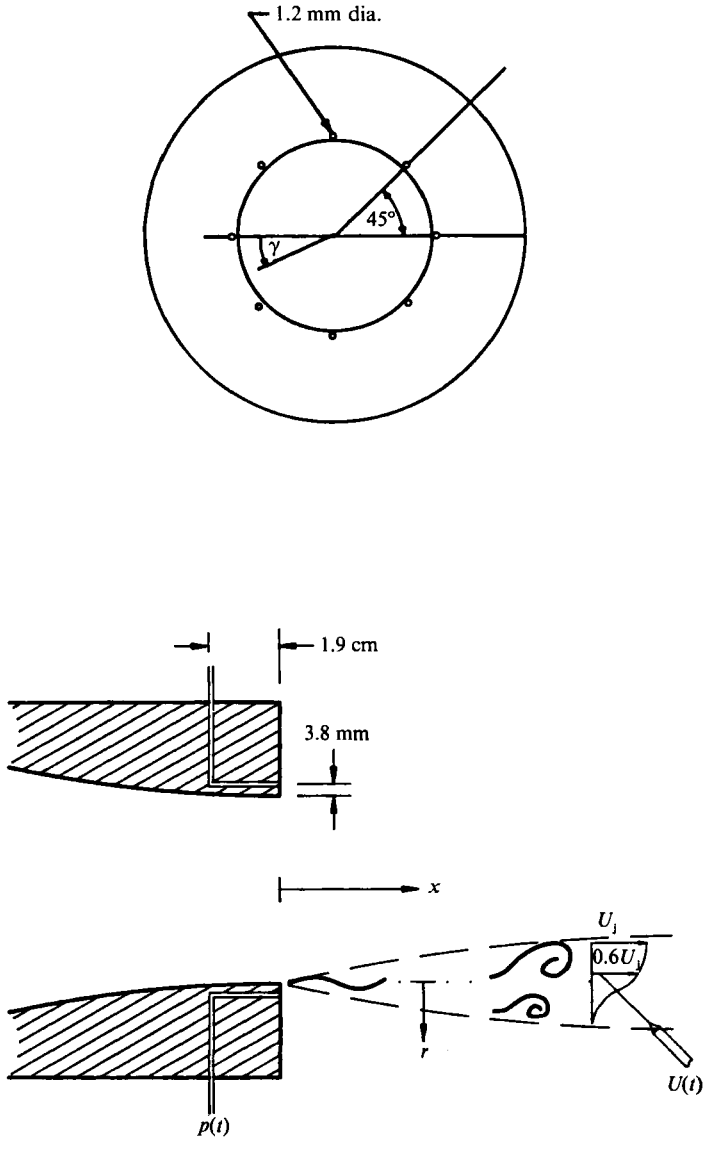

FIGURE 1. Schematic of nozzle face showing azimuthal pressure taps and laboratory coordinate system for measurements.

provide sites for measuring the unsteady pressure field near the separation point at the jet lip.

The data consisted of simultaneously acquired time series of the unsteady pressures at the lip of the jet, and the streamwise velocity fluctuations measured at different spatial locations in the shear layer, up to approximately one diameter downstream. The velocity samples were always taken at the same azimuthal position as the sampled pressure port. This arrangement is sketched at the bottom of figure 1. A voltage proportional to pressure was obtained from a B&K Type 2209 precision sound level meter which provided a flat amplitude response up to approximately 4000 Hz. A hot wire powered by a DISA 55D01 constant-temperature anemometer

provided a voltage related to the streamwise velocity component. These analogue voltages were DC biased and amplified before being digitally sampled and stored on digital magnetic tape.

For the forced jet cases, an upstream-oriented acoustic speaker was placed 4 m downstream on the jet centreline. Pure tone oscillations of the speaker were driven by a B&K 1022 beat frequency oscillator. The frequency and amplitude of the forcing sound were set while monitoring the unsteady pressures at the lip using an HP 3582A real-time spectrum analyzer. This was done with and without flow. The amplitude of the forcing was approximately 0.05% of the dynamic head based on the jet core velocity.

Post processing first consisted of digitally calibrating the pressure and velocity data series. For the velocity data, a fourth-order polynomial was used to linearize the anemometer output. Other processing generally involved calculating the mean and r.m.s. of the fluctuating quantities, the auto- and cross-spectra and coherence based on long and short time segments using fast Fourier transforms and maximum entropy spectral estimations, respectively, and the auto- and cross-bicoherence. Greater details on the more specialized statistical techniques are presented in the following sections.

3. Mode energy distributions

This section documents the streamwise development and the radial dependency of the instability eigenmodes in the initial shear layer of the circular jet. These results encompass the region starting from the lip of the jet, downstream through the first pairing location, and radially across the shear layer. For the dominant instability modes, the modulus of the eigenmodes was calculated from the spectral amplitude of the streamwise velocity fluctuations. The phase of the eigenmodes was determined from the pressure–velocity cross-spectrum. The phase measurements were relevant since the linear coherence between the velocity fluctuations in the near-field region of the shear layer and the pressure fluctuations at the lip of jet were high valued for the principle instability modes.

The bulk of the results are presented as two-dimensional contour plots, with the x-axis representing the streamwise direction, starting from $x/D = 0.05$, and the y-axis representing the radial direction normalized by either the jet diameter or the local momentum thickness. The contour plots are oriented or show the core of the jet on the top of the plot and the ambient field on the bottom. In order to obtain a better continuous spatial distribution of the plotted quantities, the discrete value points were spline-fitted first in the radial direction and next in the streamwise direction. A very low damping coefficient was used in the spline fit in order to not alter the actual data values. The constant-level contour plots were generated from these spline-function fits.

3.1. *Jet mean characteristics*

The two-dimensional contour mapping of the local mean velocity normalized by the jet exit velocity for the low initial disturbance level, 1L case, at $Re = 42000$ is shown with a physical radial coordinate in figure 2(a). It is apparent from this figure that upstream of $x/D = 0.30$, the shear layer barely spreads from its initial thickness. The first significant growth of the shear-layer thickness occurs at approximately $x/D = 0.40$. The rate of spreading further increases at approximately $x/D = 0.60$. We shall verify later that these positions correspond respectively to the points of energy saturation of the fundamental and subharmonic axisymmetric modes. We expect

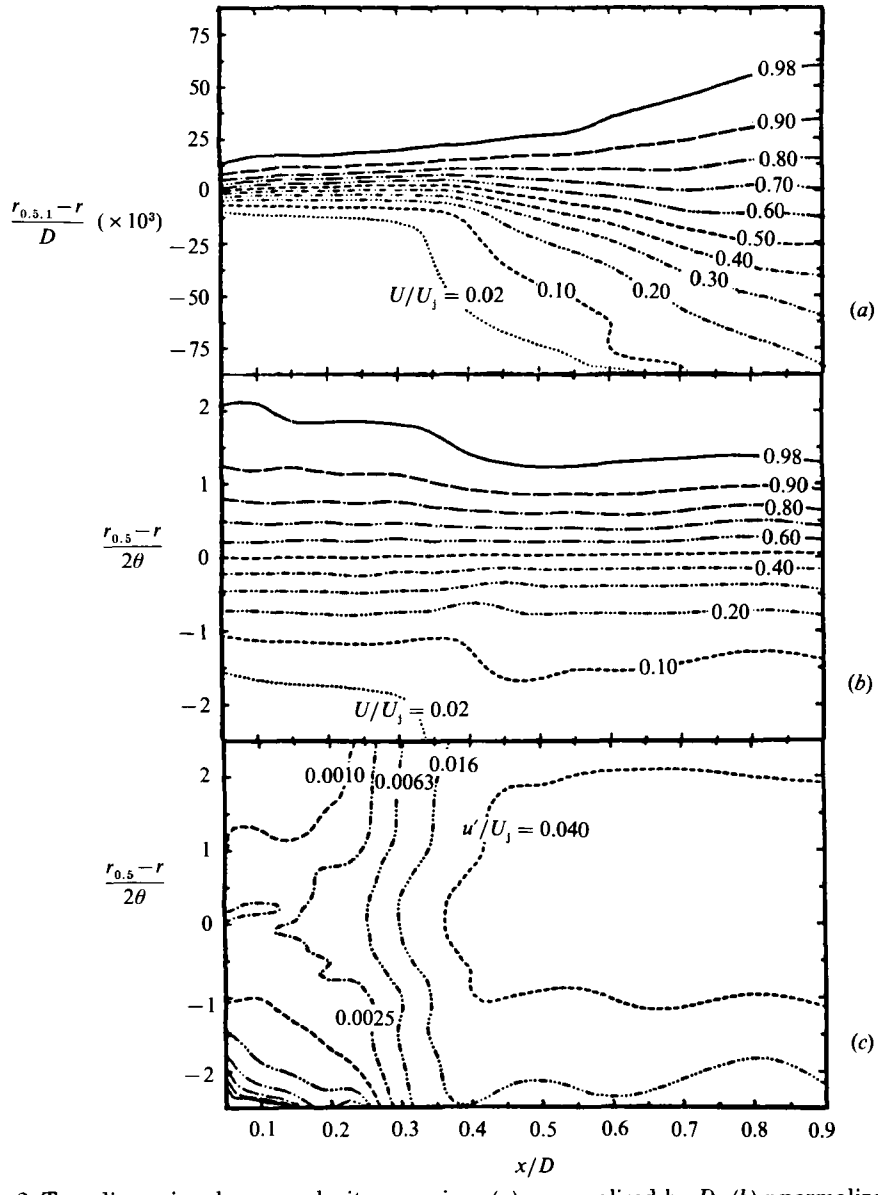

FIGURE 2. Two-dimensional mean velocity mapping: (*a*) r normalized by D; (*b*) r normalized by θ; and (*c*) r.m.s. velocity mapping in logarithmic scale with r normalized by θ ($Re = 42000$, 1L case).

that these x-locations should also coincide with the points of first vortex roll-up and vortex pairing and that the local changes in the shear-layer growth are attributable to these energetic motions.

The iso-mean velocity lines in figure 2(*a*) are reproduced in figure 2(*b*) with the radial coordinate now normalized by the local momentum thickness, $\theta(x)$. This demonstrates that self-similar mean flow behaviour exists, even well past the point of pairing in this jet.

For the same jet condition, the two-dimensional contour mapping of the total r.m.s. of the streamwise velocity fluctuations normalized by the jet exit velocity is shown in figure 2(*c*). The radial coordinate is again normalized by $\theta(x)$. The r.m.s.

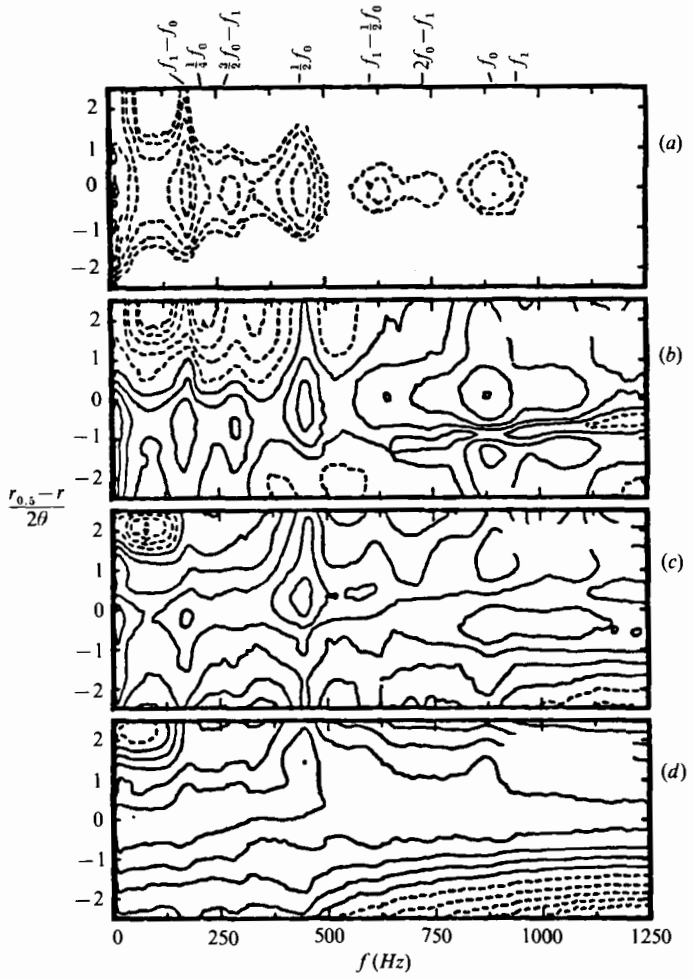

FIGURE 3. Radial spread of velocity power spectra, in logarithmic scale ($Re = 42000$). (*a–d*) $x/D = 0.15, 0.35, 0.55\ 0.80$ respectively. 5 dB beween each contour line.

values are plotted on a logarithmic scale in order to highlight regions of exponential growth.

3.2. *Dominant eigenmodes*

The radial spread of the power spectra of streamwise velocity fluctuations for this case at four downstream locations are shown in the contour plots of figure 3. The amplitude of the spectra is plotted on a logarithmic scale with 5 dB difference between the contour levels. To differentiate the amplitude levels easily, the six highest levels are plotted as solid lines and the next five levels as dashed lines. From this and similar plots the dominant instability and interacted modes are identified. The fundamental axisymmetric mode, designated f_0, occurs at 880 Hz. Although not as apparent in this presentation, the other fundamental mode for this Reynolds-number jet occurs at 1050 Hz and corresponds to the $m = \pm 1$ helical mode. This frequency is designated f_1. The other spectral peaks correspond to sum and difference modes derived from the initial fundamental modes. These include $\frac{1}{2}f_0$, f_1-f_0, f_0-f_1, $f_1-\frac{1}{2}f_0$, $2f_0-f_1$ and $\frac{1}{4}f_0$.

The evidence that the 1050 Hz mode at this Reynolds number is the fundamental

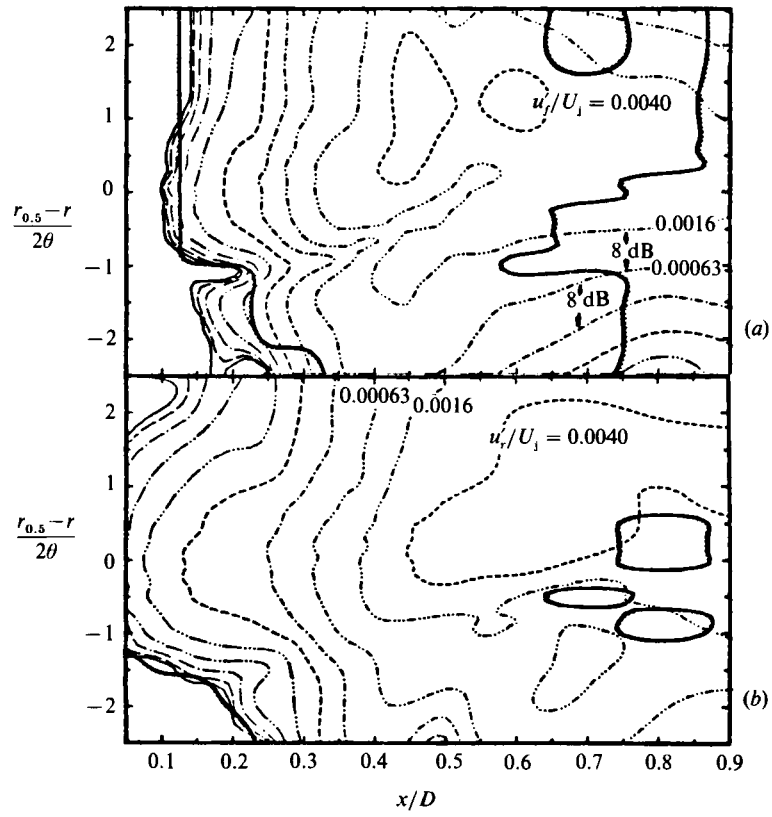

FIGURE 4. Two-dimensional spectral amplitude mapping of initial (*a*) axisymmetric and (*b*) subharmonic modes, with r normalized by θ ($Re = 42000$, 1L case).

$m = \pm 1$ helical mode comes from two sources. The first is the investigation of Drubka (1981), which was performed for the same jet and Reynolds numbers. His measurements were made using a velocity sensor at a fixed position in the shear layer, and a pressure sensor monitoring the simultaneous unsteady pressure at different azimuthal positions on the exit lip. These produced quantitative documentation of the 180° azimuthal phase change associated with the $m = \pm 1$ helical mode occurring at this frequency. The frequency associated with the axisymmetric mode , f_0, showed no azimuthal phase change. These results have also recently appeared in the paper by Drubka, Reisenthal & Nagib (1989), in their figure 10.

Other evidence comes from the analysis of Mattingly & Chang (1974), who examined the linear stability of axisymmetric jets with exit shear layers which were thin compared to the jet radius. They found that both the axisymmetric and $m = \pm 1$ helical modes had nearly the same amplification rates, and occurred at frequencies which differed by approximately 20%. Recent measurements by Kusek, Corke & Reisenthel (1990) have documented in this jet, for $22500 \leqslant Re \leqslant 90000$, a constant Strouhal number, St_θ, for the three dominant modes, f_0, f_1 and $\frac{1}{2}f_0$ (figure 6 of that reference) of 0.0144, 0.0180 and 0.0076, respectively. Based on Michalke's (1971) spatial theory, the initial most-amplified axisymmetric disturbance frequency for a hyperbolic tangent mean velocity profile corresponds to $St_\theta = 0.017$. Gutmark & Ho (1983) have tabulated values for St_θ for the fundamental axisymmetric mode from

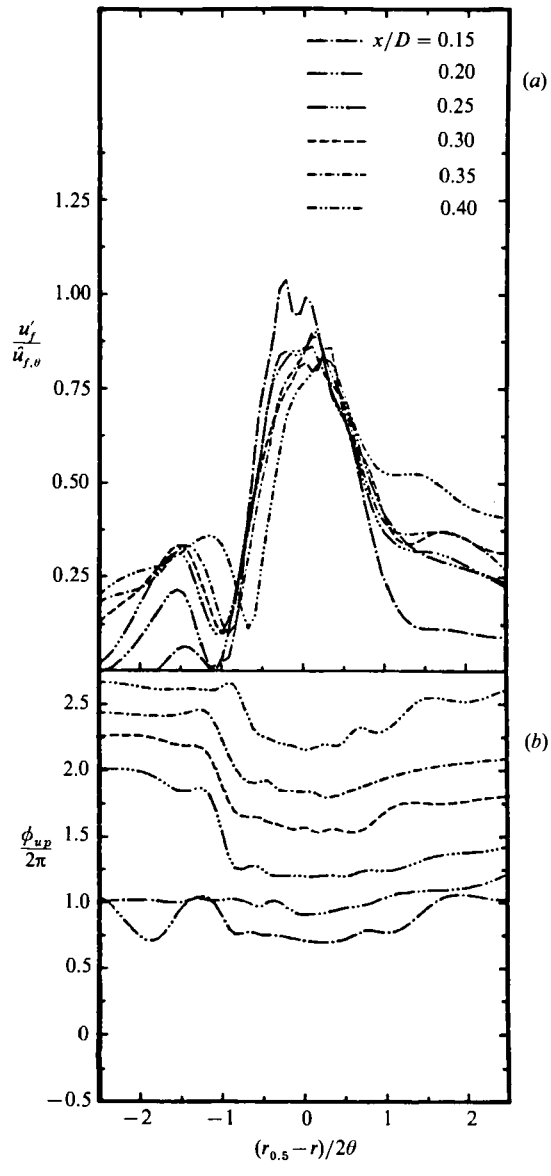

FIGURE 5. (*a*) Modulus and (*b*) phase of initial axisymmetric eigenmodes, mode f_0 ($Re = 42000$, 1L Case).

experiments in nine different jet facilities. The values they report range from 0.012 to 0.018. Our values for the axisymmetric fundamental and twice-subharmonic modes fall in the middle of this range. As theory predicts, St_θ for f_1 is 20% higher than these. Based on these results, we feel confident in identifying these fundamental modes based on their streamwise frequency alone.

We focus on the fundamental axisymmetric and subharmonic modes in figure 4. These show iso-energy lines in the (x, r)-directions, within the shear layer, of u-component fluctuations associated with each mode. This figure and others like it were constructed from the energy in spectral peaks at particular mode frequencies at the different sampled (x, r)-locations. Each mode was defined to fall within a frequency-

centred bandwidth of 54 Hz (± 27 Hz) which corresponded to 11 points in the spectrum for data acquired at 2500 Hz. Within the frequency bandwidth of a mode, the amplitude and phase were determined at the frequency having the maximum spectral amplitude. The velocity power spectrum at each probe position were closely examined to verify the existence of a spectral peak for each of the primary modes. From these results the regions where spectral peaks existed were identified. On such spatial maps of spectral amplitude, boundaries are plotted as thick solid lines each next to a dotted line pointing to the region where no distinguishable peaks were observed. The contour levels in these plots are in logarithmic, dB, increments so that equally spaced contours denote regions of exponential growth.

In the spectral map of the fundamental axisymmetric mode, figure 4(*a*), the streamwise spacing between adjacent constant-spectral-amplitude lines is invariant from $x/D = 0.15$ to 0.40, marking the linear exponential growth region. Within this x/D, in the region $-0.6 < (r_{0.5} - r)/2\theta < 0.6$, the contour spacing is relatively invariant with radial direction. This radial extent corresponds to a range of normalized mean velocity, U/U_j from 0.3 to 0.8, seen from figure 2(*b*). The amplitude of the fundamental mode reaches a maximum at $x/D = 0.45$. This is observed to occur on the core side of the shear layer. Beyond the pairing location, at about $x/D = 0.60$, the amplitude of this mode decreases slowly until it no longer exhibits a spectral peak, as indicated by the solid-dotted line boundary beyond approximately $x/D = 0.7$.

The spectral map of the subharmonic mode for this flow condition is shown in figure 4(*b*). Examination of this figure shows two regions of constant exponential growth from approximately $x/D = 0.10$–0.25 and from $x/D = 0.25$–0.50. Again in the middle portion of the shear layer, $-1.0 < (r_{0.5} - r)/2\theta < 1.0$, the contour spacing in the flow direction is nearly invariant with radial direction. The maximum energy of the subharmonic mode occurs at $x/D = 0.60$. This maximum occurs slightly closer to the centreline of the shear layer than for the fundamental mode maximum.

The eigenfunction moduli for the fundamental axisymmetric and subharmonic modes were extracted from the spectral-amplitude spatial maps such as these. This amounted to taking cuts along constant-x/D lines to generate the mode shapes shown in figures 5 and 6. In an effort to collapse these curves, the spectral amplitude $u'_f(x, r)$ was normalized by the square root of the total radial-integral energy at the mode frequency at that streamwise location. Two criteria were set in representing the eigenfunction. First, the eigenfunctions were defined only at streamwise locations where spectral peaks were observed, through the middle region of the shear layer. Second, the mode was to be undergoing exponential streamwise growth, based on values taken along the mode's maximum-amplitude line. In the case of the subharmonic and difference modes, two regions of exponential growth were identified. The eigenfunctions in both these regions were included. The second region is marked in the legend of figure 6 by an asterisk next to its streamwise x/D-location.

Based on the above criteria, the eigenfunction moduli of the fundamental axisymmetric and subharmonic modes are shown in part (*a*) of these figures. The corresponding eigenfunction phase distributions are presented in part (*b*). In the central region of the shear layer in figure 5, the fundamental eigenfunction moduli are reasonably self-similar up to $x/D = 0.40$, which is just upstream of the energy maxima for that mode. Outside the central region, the moduli reach self-similarity past $x/D = 0.25$. This location corresponds to the first emergence of the 180° phase change seen in the phase distributions at the bottom. The 180° phase shift coincides with the radial position of the minimum mode amplitude. The double-peaked

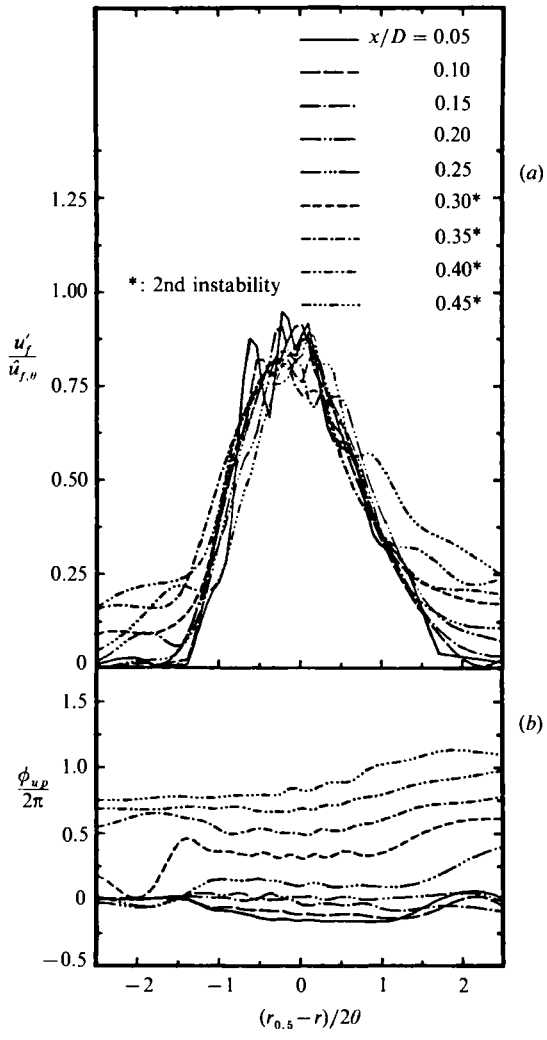

FIGURE 6. (*a*) Modulus and (*b*) phase of subharmonic eigenmodes, mode $\frac{1}{2}f_0$ ($Re = 42000$, 1L Case).

behaviour of the fundamental mode moduli and 180° phase change are consistent with the concept of a developing vorticity wave. In the middle region of the shear layer, the phase lines of the fundamental mode are approximately equidistant, indicating a constant wave velocity.

The moduli of the subharmonic eigenmodes, in figure 6, also exhibit self-similar behaviour in the central region of the shear layer. Even at $x/D \geqslant 0.30$ (asterisked positions) in the region of enhanced resonant growth, the distributions only deviate slightly. The effect of subharmonic resonance can be seen in the eigenfunction phase distribution. There we observe an abrupt increase in the streamwise spacing of iso-phase lines for $x/D \geqslant 0.30$. This corresponds to a decrease in the phase velocity of this mode, documented in a later figure, which is an adjustment to match its phase velocity to that of the fundamental mode.

In further statistics, we wish to utilize a single velocity sensor which will follow a similarity line while moving downstream. Drubka (1981) had chosen to follow the

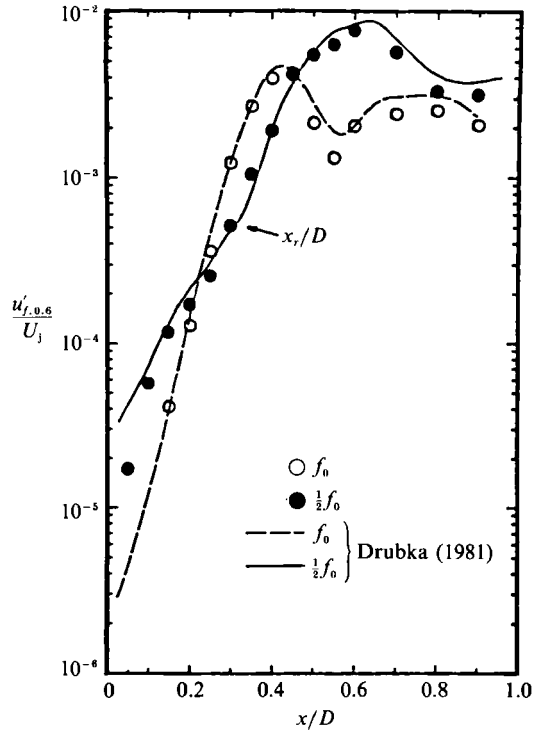

FIGURE 7. Streamwise development of initial axisymmetric mode and its subharmonic with comparison to Drubka (1981), performed in the same facility ($Re = 42000$, 1L Case, $U/U_j = 0.6$).

constant-mean-velocity line $U/U_j = 0.6$. A comparison of the streamwise growth rates for the fundamental axisymmetric and subharmonic modes determined by following this line is shown in figure 7. In this comparison, Drubka's data have been shifted to the level corresponding to a 1 Hz spectral bandwidth, which is the standard bandwidth for all our results. To investigate the sensitivity of this result to following different lines, we generated similar plots obtained while moving along the centre of the shear layer at a constant $U/U_j = 0.5$, as well as along a line which followed the mode streamwise-fluctuation maximum. The latter is shown in figure 8. Neither of these approaches takes into account the radial spreading of the shear layer. In order to capture this effect on the growth of energy in these modes, we also plotted the streamwise development of the energy in streamwise velocity fluctuations in each mode integrated radially across the layer at different x/D-locations. The results of this approach are presented in figure 9.

Comparing these first on a *qualitative* basis, we observe a number of similar features. Focusing first on the growth of the fundamental axisymmetric mode (open symbols), we observe an initial region of constant exponential growth, which eventually reaches a saturation limit at approximately $x/D = 0.45$. Past this point the energy in the fundamental mode decays. The streamwise growth of the subharmonic mode shows two regions of exponential growth. The first falls in the range from $0.15 \leqslant x/D \leqslant 0.25$ and the other from $0.25 < x/D \leqslant 0.45$. Upstream of $x/D = 0.15$, longer wavelength subharmonics are affected by the close proximity to the lip. Therefore within approximately the first quarter of the subharmonic wavelength, the amplitude levels are off the expected exponential growth rate observed downstream of this point.

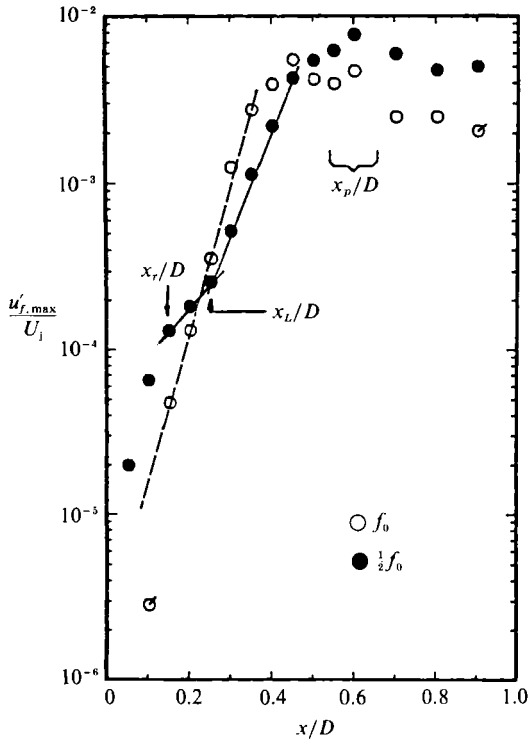

FIGURE 8. Streamwise development of initial axisymmetric mode and its subharmonic (Re = 42000, 1L Case, along each mode's maximum amplitude line). Flagged symbols: no spectral peak.

On a *quantitative* basis, regardless of the method used, the rate of exponential growth of the fundamental axisymmetric mode is virtually the same. Also, the x/D position of fundamental-mode energy saturation does not vary significantly among the four approaches. The significance of the location of the fluctuation maximum is that it marks the position of the first roll-up of the shear layer into a vortex. When scaled on the axisymmetric-mode frequency, $x/D = 0.45$ corresponds to three wavelengths from the jet lip.

For the subharmonic mode the rates within both regions of constant exponential growth are also virtually the same among the four methods. Each show the same x/D-location of 0.25 for the start of the enhanced resonant growth and, except for the similarity line $U/U_j = 0.5$, each marks the location of subharmonic energy saturation to be at $x/D = 0.6$. The first position corresponds to approximately two fundamental or one subharmonic wavelengths from the jet exit. This location coincided with the change in the phase velocity of that mode seen in figure 6(*b*) (bottom). The significance of the point of energy saturation of the subharmonic mode is that it marks the average location of vortex pairing. The characteristic position corresponds to four fundamental or two subharmonic wavelengths from the jet exit.

The streamwise phase development for these modes is shown in figure 10. These are presented along the mean velocity line $U/U_j = 0.6$ for comparison to Drubka (1981). For the fundamental mode a constant phase velocity of $0.5\,U_j$ is observed which is predicted well from linear theory. For the subharmonic mode the phase velocity in the initial growth region is the higher value of approximately $0.8\,U_j$, which is also in good agreement with linear theory. In the second growth region of the subharmonic,

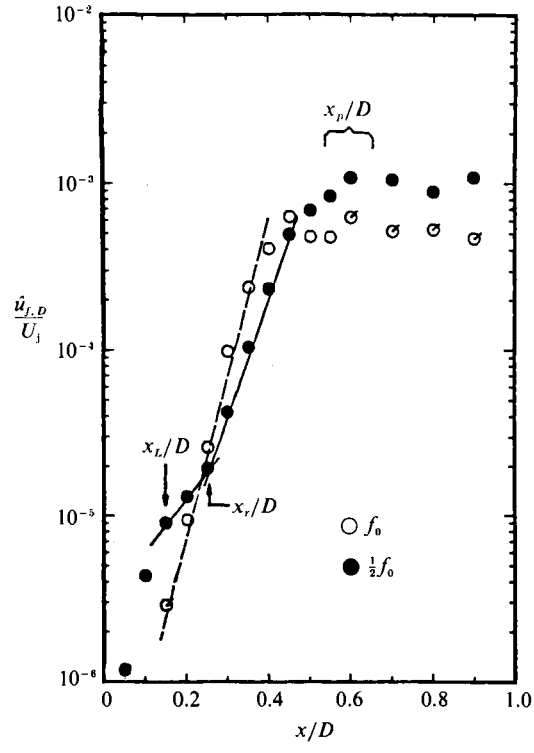

FIGURE 9. Streamwise development of radially integrated amplitude of initial axisymmetric mode and its subharmonic ($Re = 42000$, 1L Case). Flagged symbols: no spectral peak.

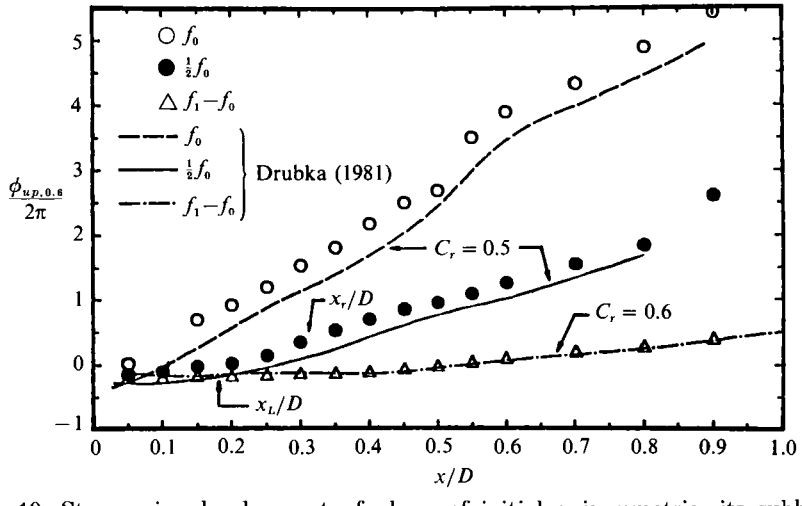

FIGURE 10. Streamwise development of phase of initial axisymmetric, its subharmonic, and difference modes ($Re = 42000$, 1L Case, $U/U_j = 0.6$).

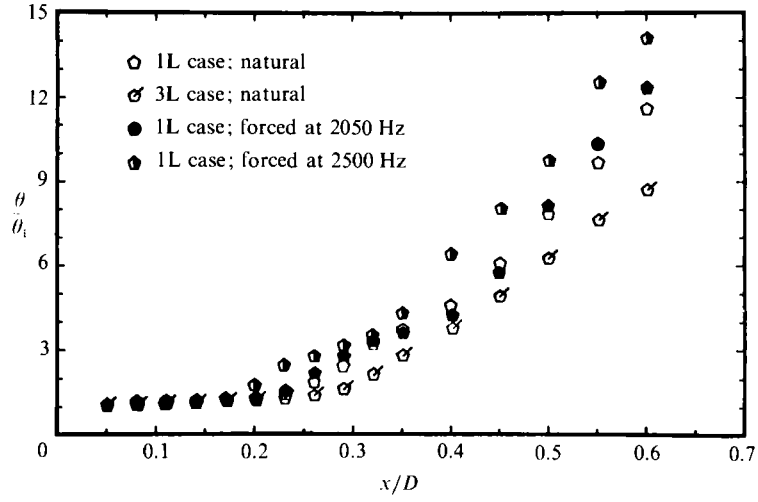

FIGURE 11. Streamwise development of momentum thickness for different initial conditions. ($Re = 70000$, natural $f_0 = 2040$ Hz).

Case	Natural 1L	Natural 3L	Forced at 2050 Hz 1L	Forced at 2500 Hz 1L
θ_i	0.0136	0.0138	0.0137	0.0142

TABLE 1. The effect of external acoustic forcing and initial core broadband disturbance level on the initial momentum thickness (in cm), for the jet at $Re = 70000$.

the phase velocity has reduced significantly to match that of the fundamental mode. The matching of the phase velocities is a prerequisite for resonance of the type predicted by Kelly (1967).

3.3. *Effect of initial conditions on dominant eigenmodes*

The remaining figures document the effect of mild axisymmetric forcing at the observed natural frequency f_0, and at a frequency 25% higher, on the development of the initial dominant eigenmodes and their interacting modes. In addition to the pure tone forcing, the effect of broadband disturbances obtained by increasing the core turbulence level is also presented. The forcing was performed at $Re = 70000$ so that in the natural condition it also provides a comparison to the previously documented $Re = 42000$ case which was known to exhibited the special jet column coupling.

The effects of the mild external acoustic forcing and the initial core disturbance level on the growth of the momentum thickness of the jet at $Re = 70000$ are shown in figure 11. The initial momentum thicknesses used to normalize the growth were measured at $x/D = 0.05$. These values are summarized in table 1.

From table 1, it is apparent that the initial momentum thicknesses did not vary significantly from one case to the other. This would indicate that even in the presence of these changing initial disturbance conditions, the frequencies of the most unstable modes, which scale with the initial shear-layer thickness, remain unchanged.

Figures 12 and 13 document the spatial distribution of fundamental axisymmetric and subharmonic mode energy in streamwise velocity fluctuations within the shear layer to $x/D = 0.6$ for the different initial states. The natural case can be directly compared to its lower-Reynolds-number counterparts in figure 4(*a*, *b*). In doing so, one must account for the shorter development length which scales with the ratio of the fundamental frequencies and core velocities. Based on these, the development length for the $Re = 42000$ 1L case is 1.40 times longer than that of the $Re = 70000$ 1L case. This has been taken into account in the scaling of the ordinate to allow these two cases to be overlayed for comparison. For such a comparison, the spatial energy distributions for the fundamental and subharmonic modes in the 1L conditions at the two Reynolds numbers are quite similar. Although we expected this based on the linear instability of the initial shear layer, it was not certain if some differences might arise owing to the special nature of the $Re = 42000$ case. Comparison of these two cases shows that the added effect of this final frequency coupling on the global energy distribution in f_0 and $\frac{1}{2}f_0$, in the initial region up to the point of first pairing, is minimal.

The immediate effect of pure tone forcing at the natural fundamental axisymmetric mode frequency of 2050 Hz and at a 25% higher frequency of 2500 Hz is to increase the initial amplitude of these modes at the jet exit, but not to greatly affect the global energy development. At the higher frequency, the development length shortens by an amount commensurate with the shorter wavelength of the unstable mode.

We do however observe some interesting differences in the subharmonic mode development with the mild pure tone forcing at the natural f_0. This is manifest in the increase in the size of the region, in the vicinity of the jet exit, where we could not detect a spectral peak (heavy line border) at the subharmonic frequency. In the unforced (natural) cases at both Reynolds numbers, the initial amplitude of the subharmonic had always been larger and more defined than that of the fundamental. This, we shall demonstrate, is a result of downstream feedback in the form of acoustic waves produced during pairing. The mild forcing at f_0 appears to inhibit this feedback process. Mild forcing at the higher frequency does not exhibit this characteristic so that the 'subharmonic' $\frac{5}{11}f_0$ mode exhibits a strong peak throughout the shear layer near the jet exit. A broadband increase in the core disturbance is observed to mask spectral peaks in the initially weaker fundamental axisymmetric mode at the jet lip, but not that of the subharmonic. The x-development qualitatively follows that of the natural low-core-disturbance cases.

The eigenfunction modulus and phase of streamwise velocity fluctuations for the fundamental and subharmonic modes at the higher Reynolds number, low initial disturbance condition were quite comparable to the lower-Reynolds-number equivalents in figures 5 and 6, and therefore are not reproduced here. The streamwise growth of these two modes is shown in figure 14. Here we have chosen to follow the line of maximum streamwise velocity fluctuations of each mode, which was shown to be representative of the whole shear layer in previous figures. Comparing this figure to its lower-Reynolds-number counterpart in figure 8, we observe the same stages of development, namely a constant exponential growth region for the fundamental axisymmetric mode, an initial and secondary exponential growth region for the subharmonic mode, and respective saturation locations at x/D-values corresponding to three and four fundamental mode wavelengths from the jet exit. The spatial growth rates of the fundamental and initial subharmonic are virtually the same for the two Reynolds numbers when scaled by their wavelengths, although the secondary subharmonic growth is somewhat higher at the higher Reynolds number.

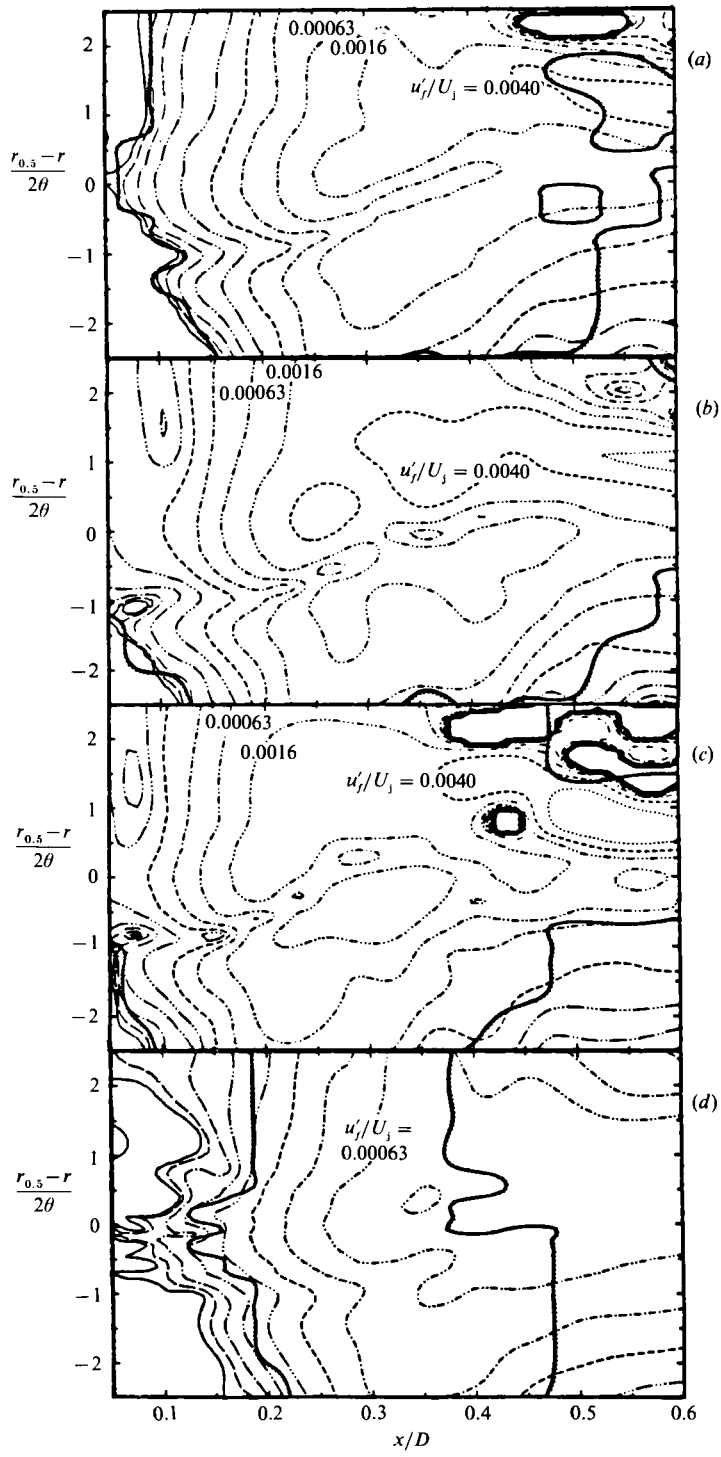

FIGURE 12. Map of spectral amplitude levels of initial axisymmetric mode for different initial conditions at $Re = 70000$. (*a*) 1L condition, (*b*) forced at 2050 Hz (*c*) forced at 2500 Hz, and (*d*) 3L condition).

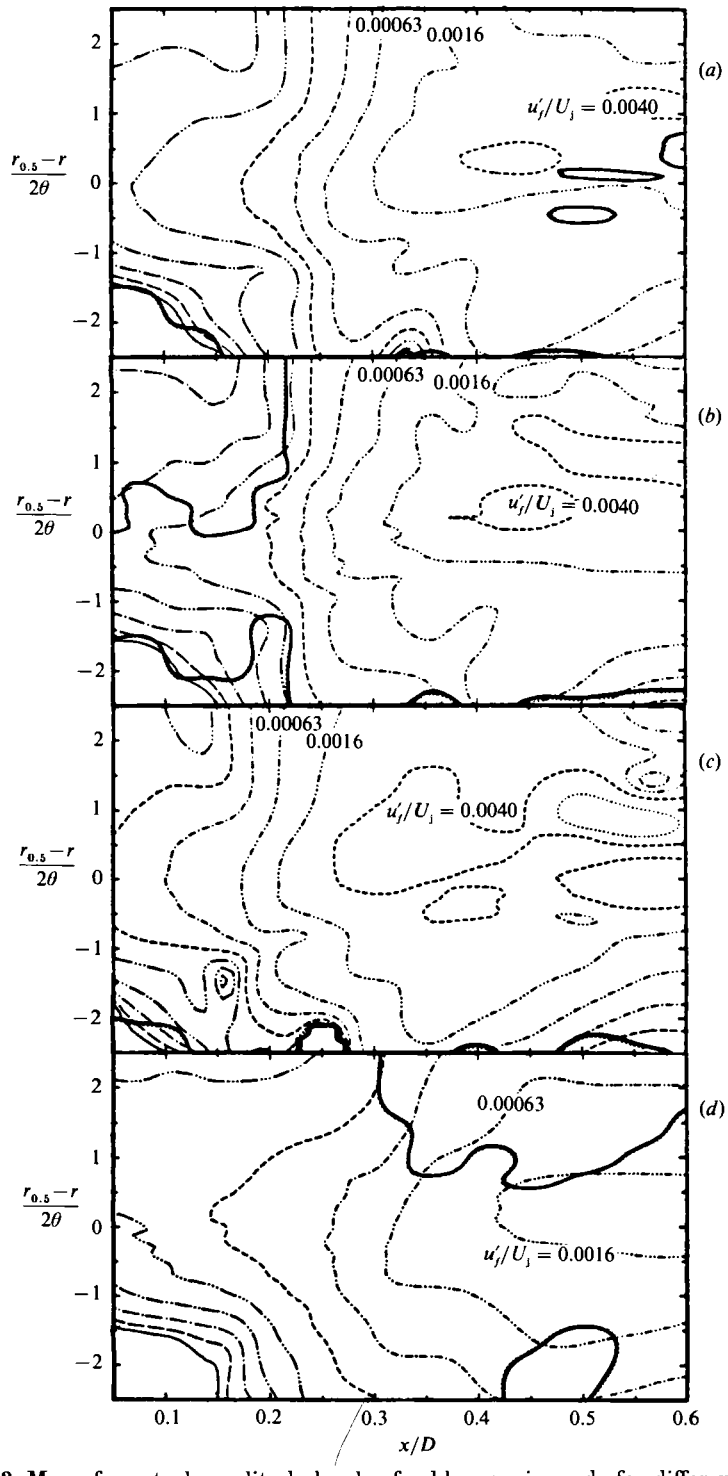

FIGURE 13. Map of spectral amplitude levels of subharmonic mode for different initial conditions at $Re = 70000$. (*a*) 1L condition, (*b*) forced at 2050 Hz, (*c*) forced at 2500 Hz, and (*d*) 3L condition.

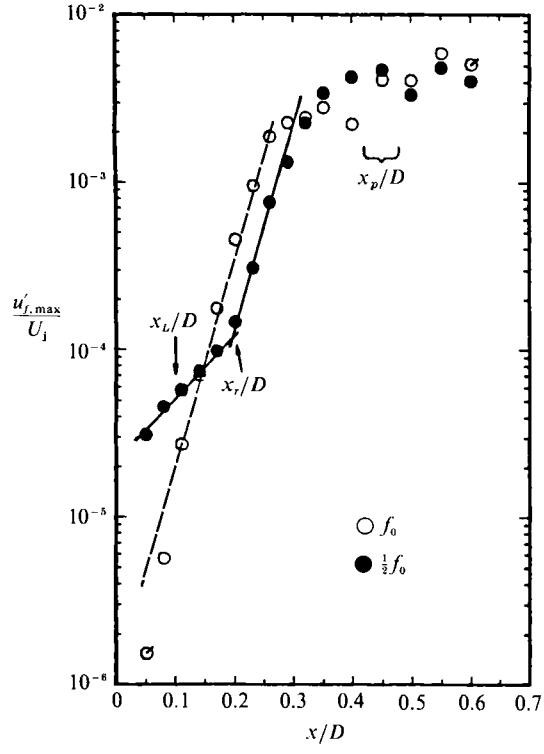

FIGURE 14. Streamwise development of initial axisymmetric mode and its subharmonic (Re = 70000, 1L case, along each mode's maximum amplitude line). Flagged symbols: no spectral peak.

At this higher Reynolds number, a spectral peak at the initial $m = \pm 1$ helical mode frequency was more discernable. We therefore plotted in figure 15 the streamwise growth of that mode, as well as the difference mode, $f_1 - f_0$. Focusing on the former, we observe a constant-valued exponential growth with a spatial rate that is the same as that of the fundamental axisymmetric mode. The comparable growth rates of these two modes had been predicted by Michalke (1971).

The difference mode is observed to exhibit two different regions of exponential growth, like that of the subharmonic mode. The x/D-location of the change in spatial amplification of the $f_1 - f_0$ mode also coincides with that point in the subharmonic growth. This would suggest a form of interaction between these modes which we shall expand upon in a later section.

With mild forcing at the fundamental axisymmetric mode frequency, the initial amplitude of that mode, seen in figure 16, has increased by approximately a factor of ten. The initial amplitude of the subharmonic remains the same. These growth curves show the same characteristic features, although the point of change of slope in the subharmonic growth is not nearly as sharp as in the natural cases. In addition, the loeation of subharmonic energy saturation has moved slightly downstream. The location of the subharmonic maximum for the natural case is marked on this figure as x_p/D.

When the jet is mildly forced at a frequency 25% higher (2500 Hz) an exact fundamental/subharmonic combination was not found to exist. Instead, near-subharmonic modes at frequencies of $\frac{5}{11}f_0$ and $\frac{6}{11}f_0$ were observed, as well as a difference combination at $\frac{1}{11}f_0$. We have speculated that the initial 'subharmonic'

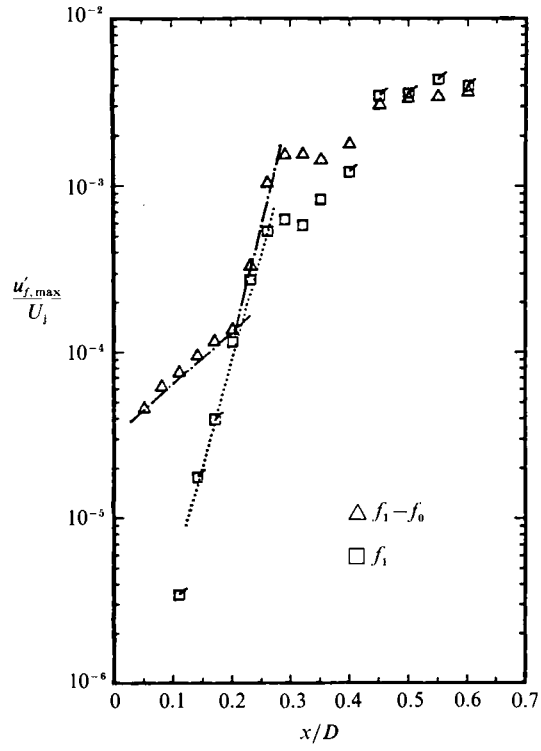

FIGURE 15. Streamwise development of difference and helical modes ($Re = 70000$, 1L case, along each mode's maximum amplitude line). Flagged symbols: no spectral peak.

mode was at the $\frac{5}{11}f_0$ frequency. Part of the basis of that speculation is contained in the eigenfunction magnitude and phase distributions in figure 17 and in the x-growth of the maximum streamwise velocity fluctuations in figure 18. In the former, we observe a good comparison to the subharmonic eigenfunctions for the natural jet, such as in figure 6. The streamwise growth of the $\frac{5}{11}f_0$ mode exhibits the characteristic 'subharmonic' development by the presence of two constant exponential regions, with the second having a significantly higher rate. The change in growth rate was also found to coincide with a change in phase velocity, seen in figure 17.

All this can be contrasted to the spatial characteristics of the $\frac{6}{11}f_0$ mode. The eigenfunction magnitude and phase distributions in figure 19 show some early x-similarity which is subharmonic-like, but eventually further downstream it develops two peaks and considerable scatter. This behaviour is a primary reason why we chose to present these past growth curves while following the fluctuation maximum, since for this case alone, the other approaches would not be representative. The x-growth of the $\frac{6}{11}f_0$ mode is shown in figure 20. For that mode we observe a single, constant exponential growth at a rate which is somewhat less than that of f_0. We observe no change in slope prior to saturation and no change in phase velocity characteristic of subharmonic behaviour. Energy saturation occurs at the same x/D-location for the $\frac{5}{11}f_0$ and $\frac{6}{11}f_0$ modes.

The streamwise growth of the $\frac{1}{11}f_0$ mode also seen in figure 20 shows two exponential growth regions, similar to the natural difference mode ($f_1 - f_0$) in the natural jet. Also similar is that the x/D-location for the change in growth of this difference mode coincides with the point of growth rate change of the $\frac{5}{11}f_0$

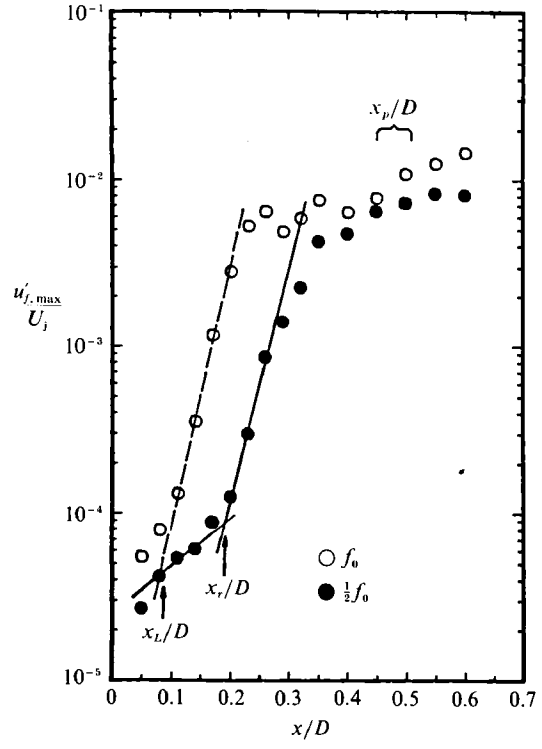

FIGURE 16. Streamwise development of initial axisymmetric mode and its subharmonic ($Re = 70000$, 1L case, (natural $f_0 = 2040$ Hz), forced at 2050 Hz, along each mode's maximum amplitude line).

'subharmonic'. We have not verified if the $\frac{6}{11}f_0$ mode is a non-axisymmetric mode, as in the case of f_1 in the natural jet.

4. Unsteady mode selection

The experimental results of Drubka (1981) had verified that a circular jet is unstable to both axisymmetric and helical modes. He had speculated, based on flow visualization, that in the initial region, $x/D < 1$, the natural jet alternates between these two modes. The answer to this speculation defines one of the principal objectives of our study. Further, the documentation of the unsteady behaviour and the effect of low-level harmonic forcing on the unsteady characteristics of the jet are also addressed with the use of short-time spectral estimations.

The methods used for studying jet instabilities, such as those of Drubka (1981), are typically based on long-time-average statistics. For example, the spectral estimations determined from discrete Fourier transforms (DFT) are usually based on the assumption that the correlation function of each data ensemble asymptotes to zero by the end of the sampling interval. This limits the minimum amount of time lag required for proper spectral estimation. The random noise introduced by the use of DFT also requires averaging of ensemble spectra or frequency smoothing. This creates a major problem. Any alternate switching of the jet instability modes from axisymmetric to helical may occur in an unsteady and non-periodic manner. The long-time statistics required for the convergent estimation of the spectral function

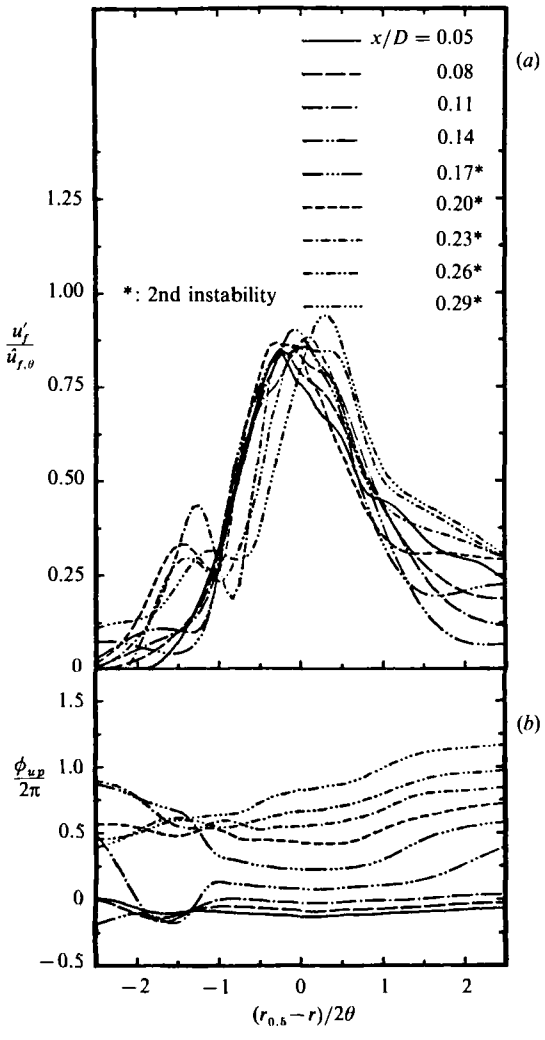

FIGURE 17. (*a*) Modulus and (*b*) phase of $\frac{5}{11}f_0$ eigenmodes (Re = 70000, 1L case, forced at 2500 Hz).

using DFT will act to mask this switching process by producing two apparent coexisting peaks at frequencies corresponding to these two modes. In addition, any slight time-variation in the mode frequencies would result in a broadening of the spectral peaks. Because of these manifestations of standard DFT processing methods, we computed short-time single-realization spectral estimates using the maximum entropy method (MEM). A description of the method is presented in Appendix A. The discussion of the results for different initial conditions in the jet are presented in the following.

4.1 *Results of unsteady mode analyses*

The *short-time* instability behaviour of the three naturally developing and two harmonically forced jets are presented in what follows. For each case, a series of short-time MEM power spectra were calculated for the simultaneously sampled pressure and velocity fluctuation data series in the shear layer at the radial position

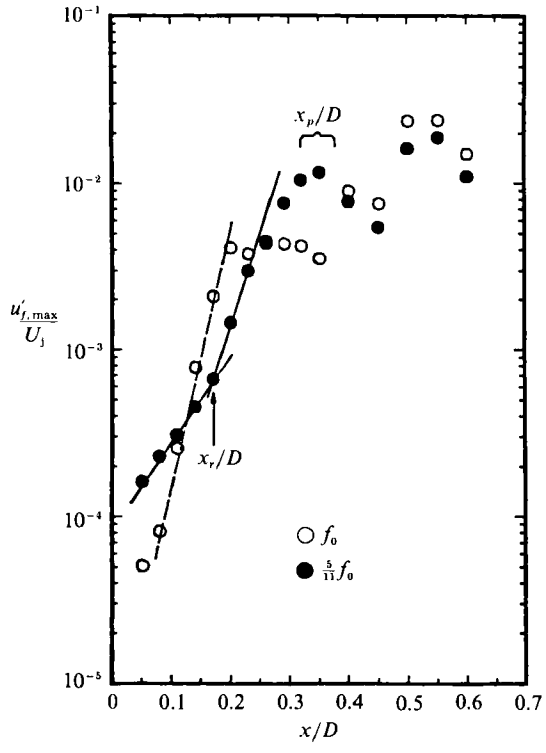

FIGURE 18. Streamwise development of initial axisymmetric and $\frac{5}{11}f_0$ modes ($Re = 70000$, 1L case (natural $f_0 = 2040$ Hz), forced at 2500 Hz, along each mode's maximum amplitude line).

$U/U_j = 0.6$. The amplitude and phase eigenfunctions of these modes shown previously, documented the x-similarity of that location. For each flow condition, and at each downstream location, consecutive MEM power spectra were calculated from contiguous overlapping short-time-series segments. It was found that 18 time-series points would result in appropriate short-record MEM spectra for the cases in this study. Based on the data sampling frequency, these 18-point records correspond to approximately five to eight axisymmetric wavelengths (eight for the 2500 Hz forced case), or six to eight helical mode wavelengths.

Each sequential 18-point time series was formed with a 15-point overlap of the preceding record. That is, each record was advanced by only three new time-series points, corresponding to one axisymmetric wavelength, for each consecutive spectral estimate. This amount was found to produce a smooth transition between contiguous spectra of the type shown in figure 21. To obtain the most conservative spectrum with emphasis on the frequency content rather than on the amplitude, an 8-point predictive error filter length was chosen for use with the 18-point records. This consistently placed the estimate into region C of our criterion map (see Appendix A), thereby producing spectra which have the correct frequency content but may not display the proper energy content.

As a verification that the correct spectral estimates were obtained from the MEM approach, long-time-averaged spectral distributions were formed by ensemble averaging the consecutive short-time estimates. These were compared to the spectra for the same data properly computed using DFT. In all cases, little difference was exhibited between the spectra from the two methods. Although this is not a

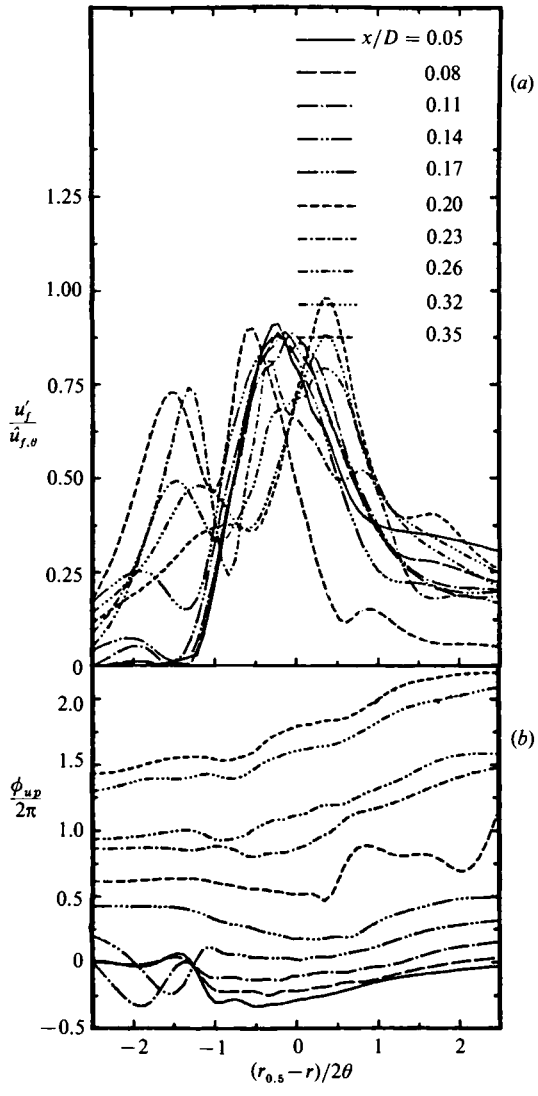

FIGURE 19. (*a*) Modulus and (*b*) phase of $\frac{6}{11}f_0$ eigenmodes ($Re = 70000$, 1L case, forced at 2500 Hz).

guarantee that every short-time spectral estimate is completely correct in all aspects, it demonstrates that a statistical majority of these have the correct frequency and amplitude information. With this degree of confidence, the results obtained by this approach are presented.

Figure 21 depicts the spectral evolution for the 1L case at $Re = 42000$ and $x/D = 0.35$. This condition was chosen to demonstrate the alternate switching between the axisymmetric and helical modes ongoing in this jet. These two modes are denoted by f_0 and f_1 at the top of the figure. The evolution can be followed in this figure; at 0 ms, when the data acquisition was started, the jet was dominated by the helical mode. This is evident by the peak at the frequency f_1. After approximately 15 ms, the emergence of the peak at f_0 marks the switching from the helical mode to the axisymmetric mode. The jet remains in the axisymmetric mode until approximately

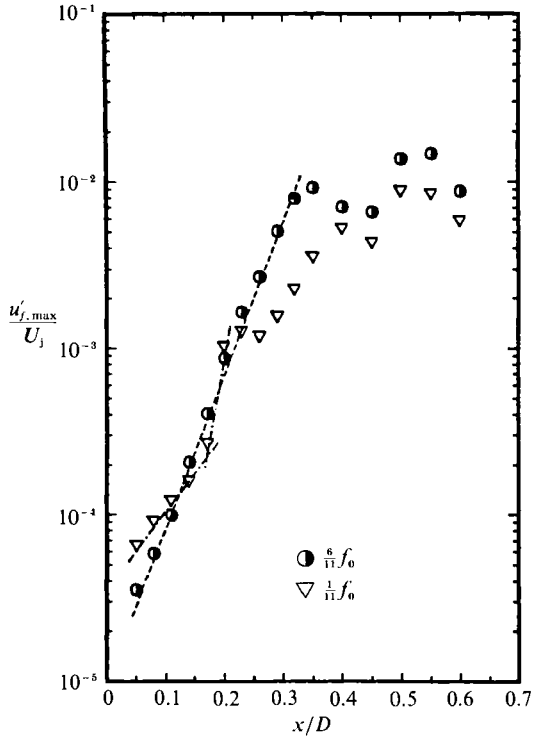

FIGURE 20. Streamwise development of $\frac{6}{11}f_0$ and $\frac{1}{11}f_0$ modes ($Re = 70000$, 1L case, natural $f_0 = 2040$ Hz, forced at 2500 Hz, along each mode's maximum amplitude line).

35 ms into the acquisition run where it shifts back to the helical mode. The alternate switching between modes is apparent throughout the time evolution depicted in this figure with both modes appearing to exist for a nearly equal amount of time. A quantitative measure of the percentage of time that each mode exists follows later in this section.

A similar alternate switching between these two fundamental modes is evident from the time evolution of spectra in figure 22, at the higher Reynolds number of 70000, for the jet with low initial disturbance level at $x/D = 0.25$. This contrasts to the evolution depicted in figure 23, which occurred when the jet was axisymmetrically forced at the frequency f_0. As expected, this forcing organized the jet instability and effectively suppressed the initial development of non-axisymmetric (helical) disturbances.

To provide a quantitative measure of the percentage of time of occurrence of these dominant modes, a method was developed to detect the existence of spectral peaks (modes). The method defined a peak to be at a frequency in the spectral distribution where its amplitude was higher than at the two neighbouring frequencies. The use of such a simple definition was made possible only because of the smooth nature of spectra obtained from the MEM approach. This was meant to detect only the existence and frequency of the spectral peaks (SP). No information or criteria about the amplitude of the peaks was deduced from this method. Employing this method on the consecutive MEM spectra of both velocity and pressure data, such as shown in figures 21–23, the percentage of time a spectral peak exists at any of the resolvable frequencies, regardless of its amplitude, was deduced. The results are presented in the

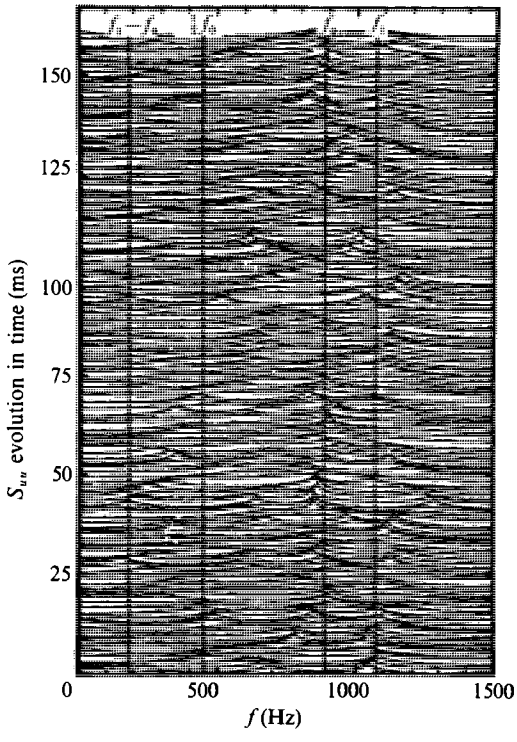

FIGURE 21. Time evolution of MEM velocity spectrum ($Re = 42000$, 1L case, $x/D = 0.35$, $U/U_j = 0.6$).

SP histograms of figures 24–28. These were constructed from 2000 consecutive MEM spectra in order to be representative of the overall spectral peak distribution.

The spectral peak histograms of the pressure fluctuations at the lip of the jet for $Re = 42000$, 1L condition are shown in the top of figure 24. The frequencies corresponding to the difference and subharmonic modes are well defined, and have a high value owing to their dominant existence in the spectrum. This mirrors the initial self-forcing of the jet due to the coherent feedback at these frequencies.

In the initial shear layer for the same jet conditions, the velocity SP histograms in figure 24 (*b*) bring out all of the dominant modes. Since the peak detection does not discriminate between amplitudes, we expected the SP histograms to be more sensitive to even the low-amplitude modes which exist a majority of the time. This was evident in this figure, where as many as six modes can be distinguished. At the location closest to the jet exit, $x/D = 0.15$, the histogram is similar to that for the unsteady pressures at the lip. Following the development downstream, we observe the strong emergence and decay of the dominant modes which reflects their evolution and interactions.

For the same jet disturbance condition at the higher Reynolds number of 70000, the velocity SP histograms in figure 25 reveal a more consistent existence of the growing dominant modes. At this higher velocity, the development of the jet by this last station is equivalent to that at $x/D = 1.0$ for the previous figure. As in the lower-Reynolds-number case, the helical mode appears to exist for most of the time only at the location of the beginning of subharmonic resonance, $x/D = 0.35$ for Re = 42000; 0.25 for 70000.

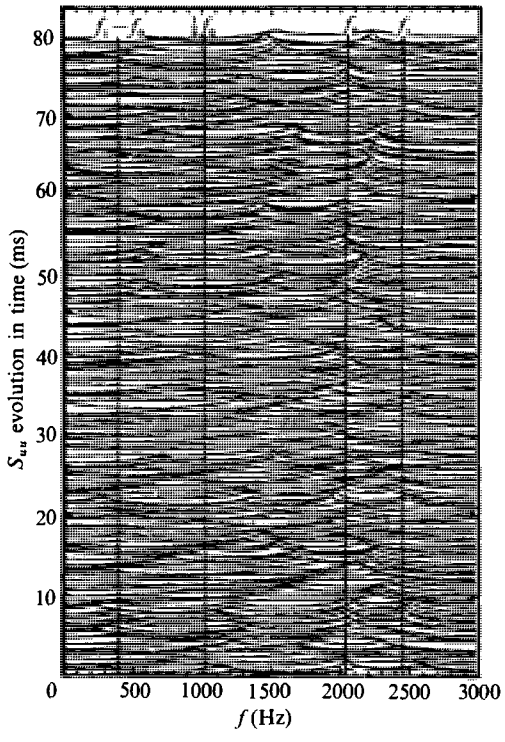

FIGURE 22. Time evolution of MEM velocity spectrum ($Re = 70000$, 1L case, $x/D = 0.25$, $U/U_j = 0.6$).

The effect of low-level forcing at the fundamental axisymmetric mode frequency on the $Re = 70000$ jet is displayed in the velocity SP histograms in figure 26. From these, the forcing at f_0 is observed to organize the fundamental axisymmetric mode, evident by its significantly higher existence percentage. Near the lip at $x/D = 0.14$, the SP occurrence of the subharmonic is lower in amplitude and more broadly distributed than in the unforced case in figure 25. By $x/D = 0.26$ however, the forcing is observed to better organize the subharmonic mode. As seen in this figure, the helical mode was strongly suppressed by the axisymmetric forcing. Speculation on the continued existence of a mode near the difference frequency in this forced jet is taken up later.

A comparison of the SP histograms for the lip-pressure fluctuations in the forced and unforced condition at $Re = 70000$ was shown in figure 26(a). In the forced case, the SP histograms reflect the additive effects of the acoustic forcing and the downstream influence of the developing shear layer. As a result, the distribution at the forcing frequency, f_0, is very sharp and high valued with a strong suppression of adjacent frequencies. The distributions at the subharmonic and difference mode frequencies are, however, relatively unchanged. We contrast this behaviour to that for the case of the jet forced at 2500 Hz in figure 27. In this case the natural f_0 mode at 2050 Hz was strongly suppressed and replaced by a new axisymmetric mode at the 2500 Hz forcing frequency. The pressure histograms at the lip reveal a sharp distribution at the forcing frequency, as with the previous forced case. In contrast to that case, the $\frac{5}{11}f_0$ 'subharmonic' has been sharply increased in the pressure histograms. In addition, the $\frac{1}{11}f_0$ difference mode is also strongly evident. These lower

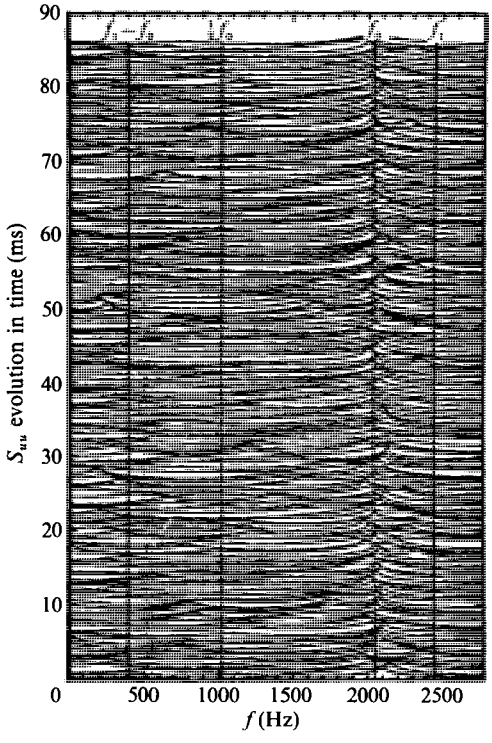

FIGURE 23. Time evolution of MEM velocity spectrum ($Re = 70000$, 1L case, forced at 2050 Hz, $x/D = 0.20$, $U/U_j = 0.6$).

frequencies are undoubtedly a result of downstream feedback. The high occurrence of $\frac{5}{11}f_0$ in the pressure signal further supports this being the axisymmetric 'subharmonic' mode for this forced jet.

The effect of higher initial disturbance levels in the core at $Re = 70000$ is presented in the SP histograms in figure 28. Comparing these to the low-disturbance case of figure 25, the higher broadband disturbances are observed to lead to less organized axisymmetric modes. In particular, an almost equal predominance of the helical mode at all streamwise locations is observed. A similar sensitivity of the helical mode to initial broadband disturbance levels was reported by Drubka (1981).

In order to form statistics on the occurrence and interaction of the different modes brought out by the MEM spectral estimates, spectral peak indicator functions were generated. For these, the frequencies corresponding to the fundamental axisymmetric mode, its subharmonic, the helical mode, and the difference mode for the jet were focused on. The frequencies corresponding to the axisymmetric fundamental mode and difference mode were identified from their predominant location in the SP histograms. The subharmonic frequency was then constrained to be half that of the axisymmetric frequency. Similarly, the helical mode frequency was constrained to be the sum of the axisymmetric fundamental and difference mode frequencies. The frequency bandwidth, within which a spectral peak would be accepted to correspond to one of these modes, was chosen as the average of the half-width of a Gaussian distribution fit of the axisymmetric and the difference mode velocity SP histograms. These bandwidths for the different modes are indicated on the SP histograms of figures 24–28.

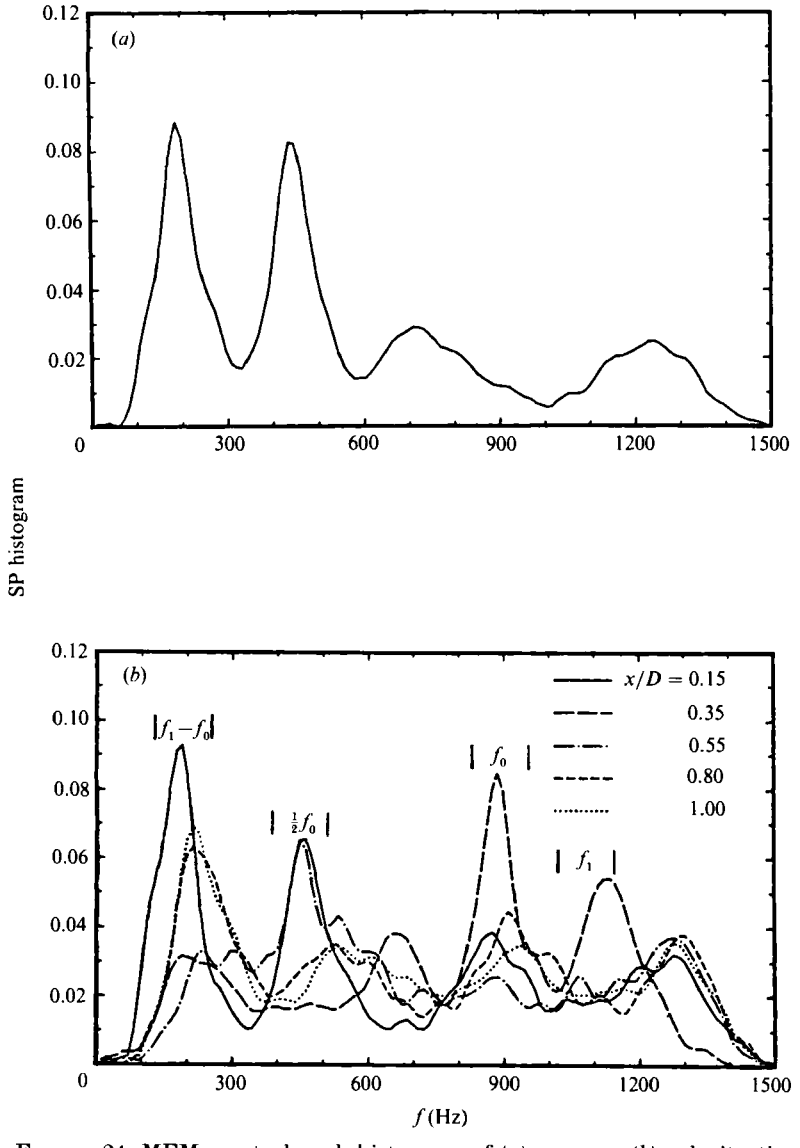

FIGURE 24. MEM spectral peak histogram of (*a*) pressure (*b*) velocity time series ($Re = 42000$, 1L case, $U/U_j = 0.6$).

If a spectral peak was observed within the frequency bandwidth of a given mode on the MEM power spectrum, that mode was considered to be present at that time. This occurrence resulted in a value of one for the indicator function for the period of time that the mode existed. A value of zero indicated the instant over which the mode was not present. The indicator functions for the different modes, at a particular jet condition, were correlated to bring out any interdependence between the evolution of the jet instabilities. The percentage of time an instability mode exists in the total time series will be equal to the average value of the indicator function. Sample indicator functions corresponding to the MEM spectral evolutions in figure 22 are presented in figure 29.

Statistical summaries of the occurrence of the four principle jet modes, taken from

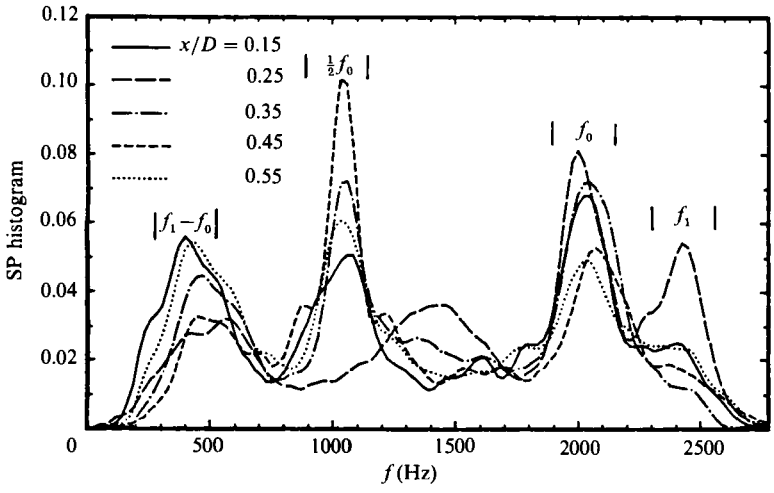

FIGURE 25. MEM spectral peak histogram of velocity time series (Re = 70000, 1L case, U/U_j = 0.6).

spectra of pressure fluctuations at the jet lip, are presented in table 2 for the different jet conditions. These statistics are based on approximately 2000 MEM spectra covering approximately 2 s of data acquisition for the Re = 42000 case and 4 s for the Re = 70000 cases. Analysis of the longest continuous data records, of 10 s for the Re = 42000 1L case, showed no significant differences in these statistics or their distributions.

The results in table 2 provide information about the disturbance field fed back from the developing velocity field. In the Re = 42000, 1L case, the occurrence of the subharmonic mode is very high. At this Reynolds number, the feedback of the subharmonic mode resulting from pairing, is significantly higher owing to the natural coupling of the initial shear layer and jet final Strouhal frequencies. By comparison, we observe that at the higher Reynolds number, where the natural coupling is not present, the subharmonic mode is significantly less dominant.

At the higher initial disturbance level condition a significant reduction in the occurrence of the subharmonic mode in the lip-pressure signal was observed. The introduction of broadband disturbances in this case has also resulted in an increase in the occurrence of the helical mode. One must be careful, however, about trying to infer to much information about the helical mode from the analysis of the pressure fluctuations at the lip, since this mode did not exhibit a strong peak in the lip-pressure SP histograms.

The occurrence of the difference mode, which shows a strong existence in the pressure signal, is only slightly reduced by the axisymmetric forcing at f_0. If the difference mode is the result of the interaction between the axisymmetric and helical modes in the shear layer, the reduction in the occurrence of the helical mode might suggest a similar reduction effect on the difference mode. This, however, was not the case.

The streamwise development of the SP occurrence for the four dominant instability modes in the velocity field of the shear layer is shown in figures 30 and 31 for the different jet conditions. We focus first on the development of the subharmonic mode in the Re = 42000 1L case, in figure 30. There, past the influence of the lip, we observe a decrease in the SP occurrence towards a minimum at x/D = 0.35. This

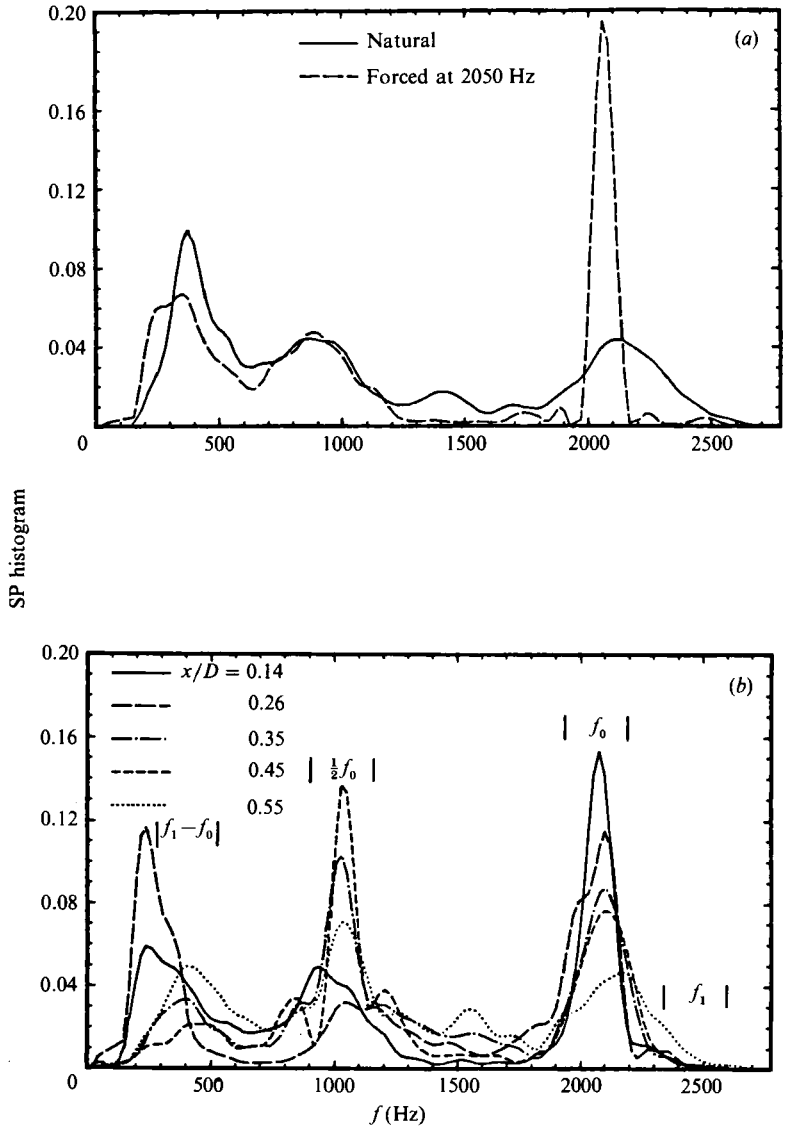

FIGURE 26. MEM spectral peak histogram of (*a*) pressure and (*b*) velocity time series (Re = 70000, 1L case, natural f_0 = 2040 Hz, forced at 2050 Hz, $U/U_j = 0.6$).

location is slightly downstream of the beginning of the subharmonic resonance. Downstream of this location, the occurrence of the subharmonic mode increases, reaching a maximum at $x/D = 0.65$. This position coincides with the subharmonic fluctuation maximum.

The occurrence development of the fundamental axisymmetric mode is almost the reciprocal of that of the subharmonic. The occurrence of this mode increases from the lip and reaches a maximum at $x/D = 0.45$, which is close to the position of maximum energy in that mode. The rapid decrease in its occurrence past $x/D = 0.45$ is associated with the rapid growth of the subharmonic mode and ultimate pairing of the formed vortices. Similar development behaviour of these modes occurs for the higher Reynolds number of 70000, 1L case, shown in figure 31 (*a*).

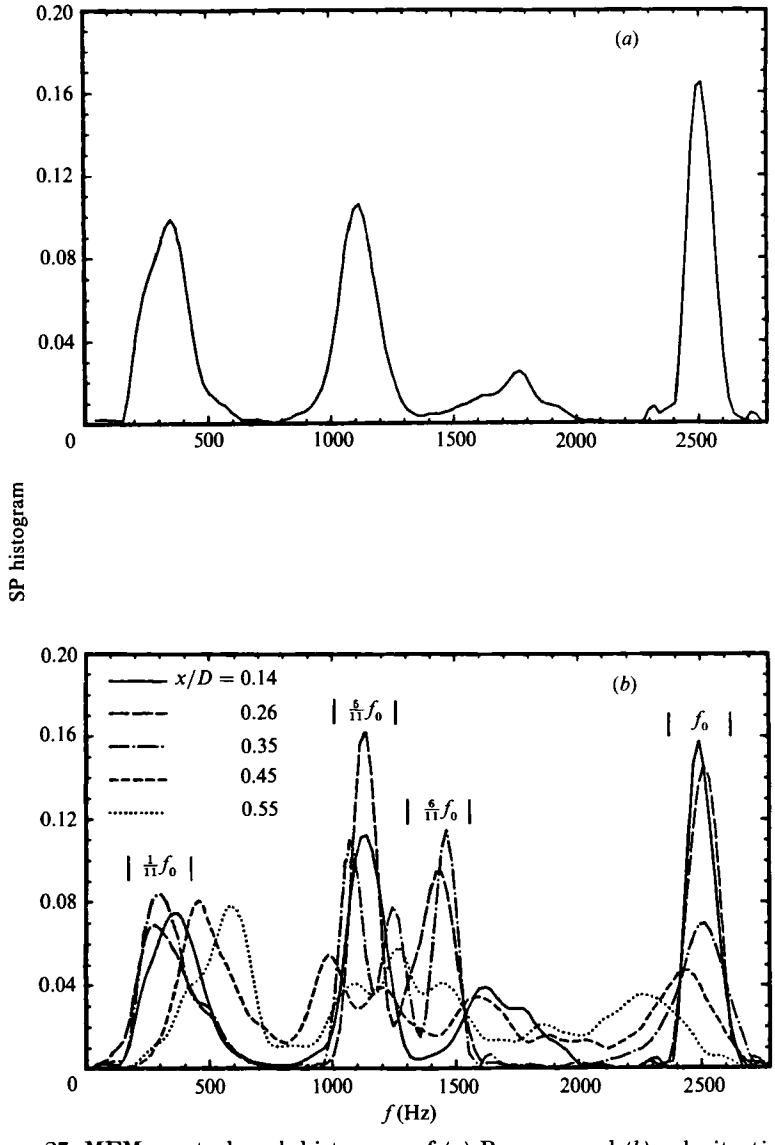

FIGURE 27. MEM spectral peak histogram of (*a*) Pressure and (*b*) velocity time series ($Re = 70000$, 1L case, natural $f_0 = 2040$ Hz, forced at 2500 Hz, $U/U_j = 0.6$).

The external acoustic forcing at the fundamental frequency has interferred greatly with the natural development of the jet as depicted by the occurrence development of the velocity SP in figure 31 (*b*). As a result of the forcing at f_0 the occurrence of this mode is initially much higher than in the natural case. After a small initial increase, its occurrence decreases towards the natural case behaviour. By $x/D = 0.35$, the energy of the axisymmetric mode has reached a maximum. At this location the forced axisymmetric mode has becomes less organized, evident by a broadening of its SP histograms in figure 26. These results reflect the diminishing influence of the low-level forcing on this mode as it develops downstream.

The forcing at f_0 has moved the maximum occurrence of the subharmonic mode slightly downstream of the natural location. Since this maximum is associated with

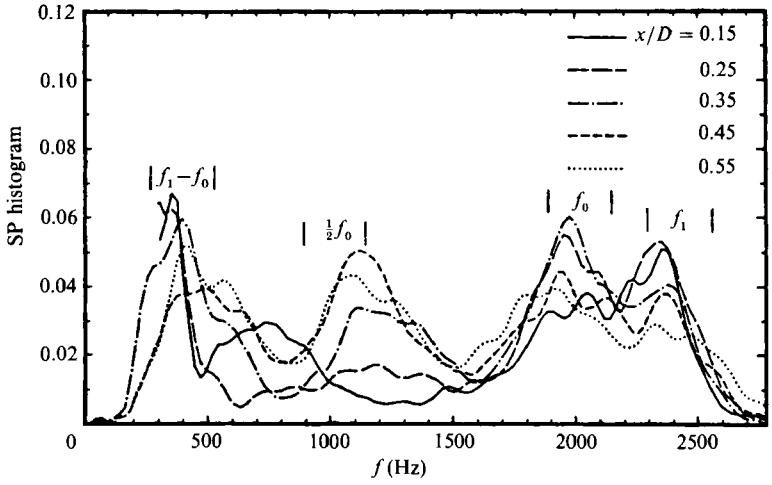

FIGURE 28. MEM spectral peak histogram of velocity time series ($Re = 70000$, 3L case, $U/U_j = 0.6$).

the pairing process, this low-level forcing appears to have slightly impeded that mechanism.

Acoustic forcing at a frequency 25% higher than the natural f_0 (figure 31*c*) has resulted in the occurrence of the forced mode reaching a maximum closer to the jet exit, $x/D = 0.25$, in proportion to the ratio of the forced frequency to the natural f_0. This case is, however, more complex than the others in that the occurrence of the $\frac{5}{11}f_0$ 'subharmonic' is a maximum upstream of the fundamental mode energy maximum. The occurrence maxima of the $\frac{6}{11}f_0$ and $\frac{1}{11}f_0$ modes bracket the locations of their energy maxima and that of the $\frac{5}{11}f_0$ mode. With the introduction of broadband disturbances in the 3L case (figure 31*d*), the occurrence of the subharmonic mode is initially lower; however, its ultimate development as well as the x-development of the other modes is comparable to the lower disturbance condition.

Focusing on the helical mode, we observe for the lower Reynolds number, 1L case that its occurrence development is approximately the reciprocal of that of the subharmonic. The helical mode is only well organized just before the onset of the subharmonic resonance. Past the pairing location its percentage time of occurrence is half the value at its peak. At the higher Reynolds number of 70000 in both the low and high initial disturbance conditions, the behaviour of the helical mode is similar to that of $Re = 42000$ case. The only difference is in the percentage values, where a greater predominance of the helical mode is observed in the higher disturbance 3L condition. The axisymmetric forcing of the jet has effectively eliminated the occurrence of the helical mode. The curious persistence of the difference mode is also evident here. In general, the streamwise development of the occurrence of the difference mode appears to follow that for the subharmonic mode, and at the furthest downstream measurement location it was the most predominant mode.

In order to present better any interdependence between the fundamental axisymmetric and helical modes, their cross-occurrence was computed from the indicator functions. The streamwise development of that quantity for the unforced jet at both Reynolds numbers is shown in figure 32. Also replotted for these cases are the auto-occurrence distributions for f_0 and f_1. If these two modes were statistically independent of one another, that is, if the occurrence of one mode was not related to

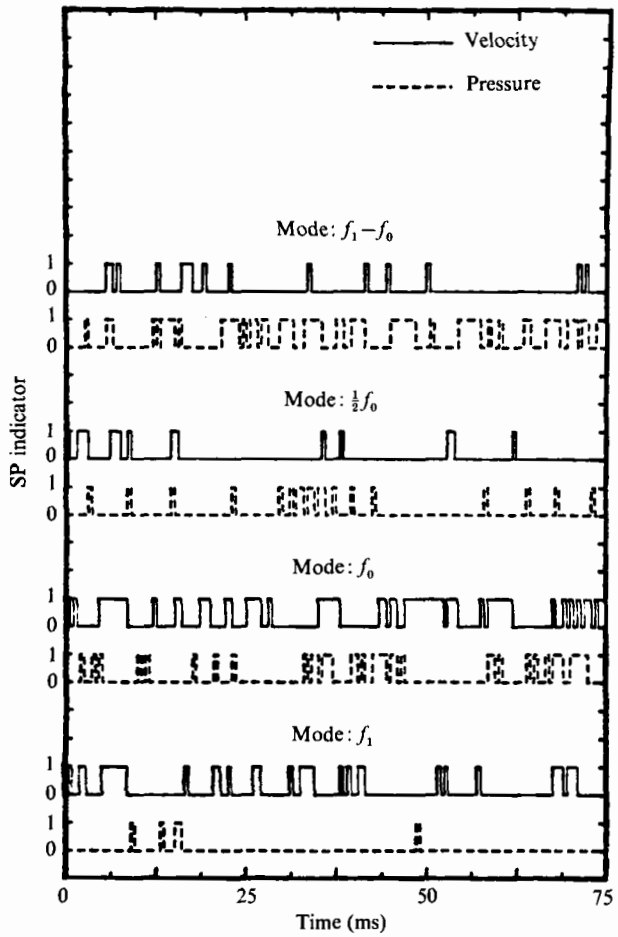

FIGURE 29. Time series of spectral peak indicator functions ($Re = 70000$, 1L case, $x/D = 0.25$, $U/U_j = 0.6$).

the occurrence of the other, their cross-occurrence would be equal to the product of their auto-occurrences. This product, signifying statistical independence, is indicated as the small-dashed line in the figure.

It is apparent here that for most of the initial region of the jet, the cross-occurrence of the fundamental axisymmetric and helical modes (indicated by the dashed-dotted line) is zero. This is true in the time series taken from both the velocity and lip-pressure data. The only location where their co-existence was not zero was at the x-position of the beginning of subharmonic resonance. The SP occurrence correlation between the axisymmetric and helical modes was also calculated and found to be consistently near zero. These results indicate that the two modes rarely coexist at the same time in the jet.

5. Nonlinear phase locking

The first- and second-order spectral estimates have been used in previous figures to determine the growth of instabilities in the jet and to document their *linear* interactions. In this section we are concerned with nonlinear, sum and difference interactions which are documented through the third-order spectrum, or bispectrum.

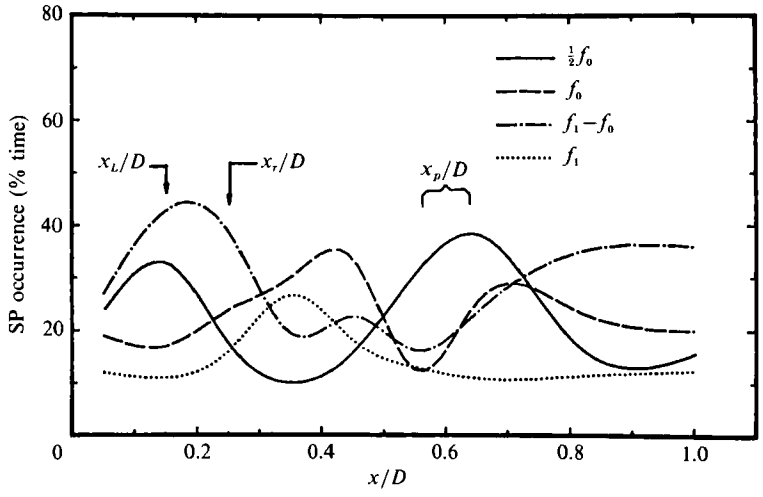

FIGURE 30. Streamwise development of spectral peak occurrence of initial axisymmetric, its subharmonic, helical, and difference modes ($Re = 42000$, 1L case, $U/U_j = 0.6$).

	Mode			
Case	f_1-f_0	$\frac{1}{2}f_0$	f_0	f_1
$Re = 42000$	45.4	35.0	6.3	6.3
Case 1L	(2.2)	(1.5)	(1.0)	(1.0)
$Re = 70000$	38.1	13.0	26.3	3.8
Case 1L	(2.1)	(1.1)	(2.9)	(0.6)
$Re = 70000$	27.7	15.3	64.4	1.8
Forced 2050 Hz	(1.2)	(1.9)	(1.6)	(0.2)
Case 1L				
$Re = 70000$	23.5	6.4	26.9	6.7
Case 3L	(1.3)	(0.5)	(2.1)	(1.2)

	Mode			
Case	$\frac{1}{11}f_0$	$\frac{5}{11}f_0$	$\frac{6}{11}f_0$	f_0
$Re = 70000$	52.0	35.5	3.8	48.8
Forced 2500 Hz	(1.4)	(2.4)	(0.6)	(1.0)
Case 1L				

TABLE 2. Spectral peak occurrence of the instability modes in the pressure field at the lip of the jet in percent of total time. (Note: The data in parentheses are the standard deviations calculated from several sets of SP indicators).

Some early references to bispectral estimates include Hinich & Clay (1968) and Hasselman, Munk & McDonald (1963) in applications to geophysical flows. Lii, Rosenblatt & Van Atta (1976) used the bispectral estimates, in conjunction with the equation for the rate of increase of energy in a homogeneous turbulent flow field, to show the source and direction of energy transfer between the frequencies. Other investigators have extended the use of bispectral estimations to study other complex nonlinear flow systems such as transition to turbulence in a two-dimensional wake (Miksad *et al.* 1982; Miksad, Jones & Powers 1983; and Solis, Miksad & Powers 1986), instability and feedback in an impinging shear layer (Kinsely & Rockwell 1981), and

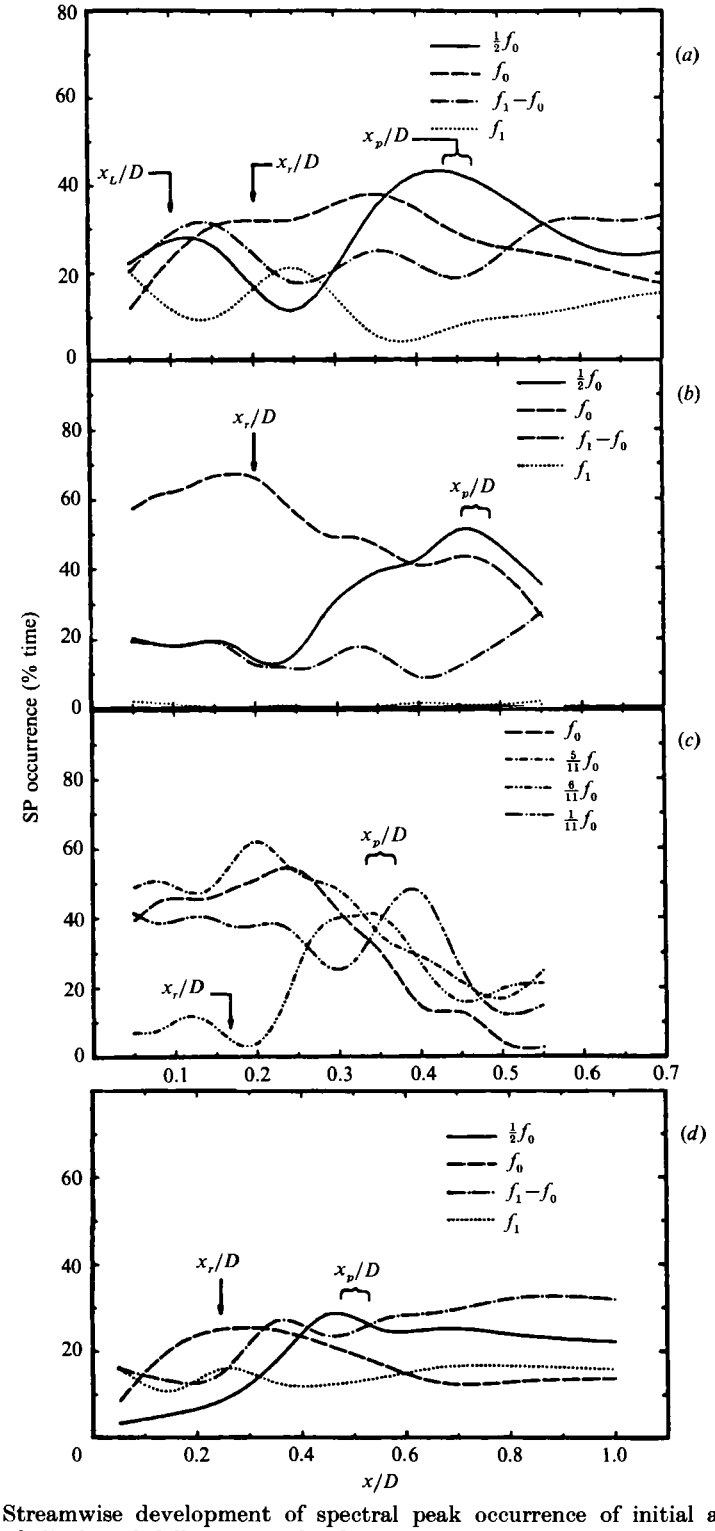

FIGURE 31. Streamwise development of spectral peak occurrence of initial axisymmetric, its subharmonic, helical, and difference modes for different initial conditions at $Re = 70000$. (*a*) 1L condition, (*b*) forced at 2050 Hz, (*c*) forced at 2500 Hz, (*d*) and 3L condition).

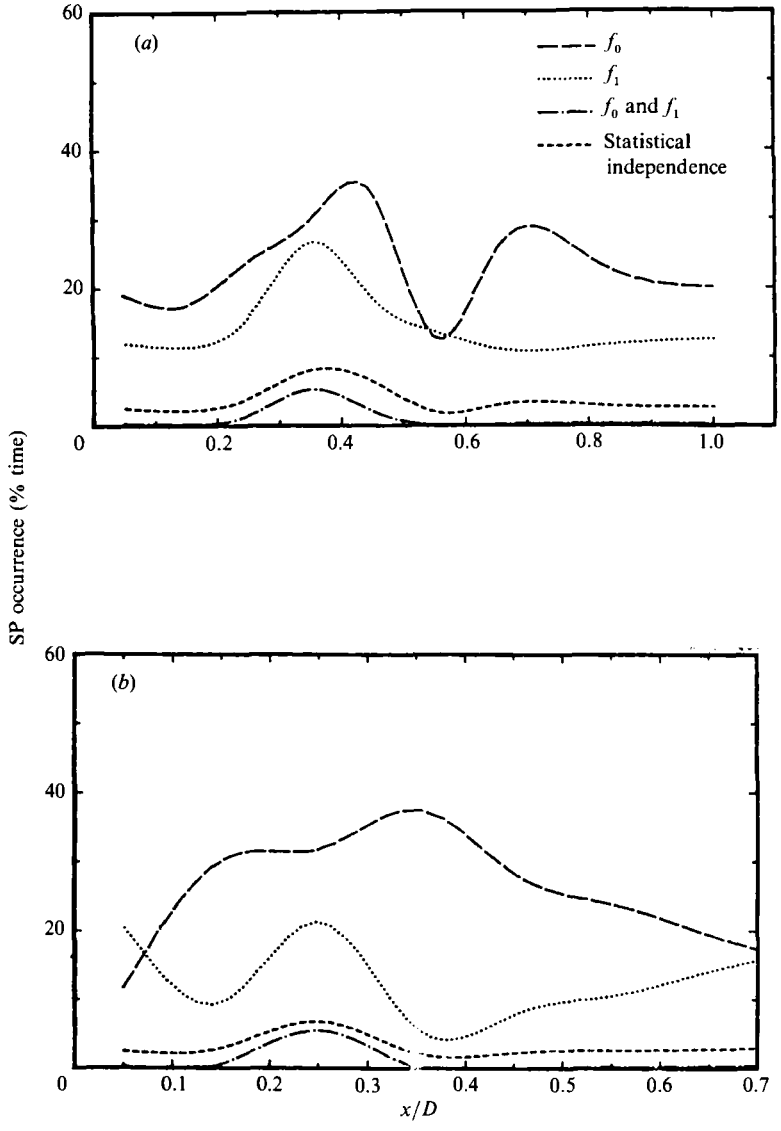

FIGURE 32. Streamwise development of cross-spectral peak occurrence of initial axisymmetric and helical modes as compared with statistical independent line for (*a*) $Re = 42000$ and (*b*) 70000 (1L case, $U/U_j = 0.6$).

in a Blasius boundary layer undergoing transition to turbulence (Corke & Mangano 1987, 1989).

In the present work the bispectral estimates were utilized to measure and document the nonlinear interactions which are a part of the initial shear-layer instability, vortex formation, vortex pairing and feedback in axisymmetric jets. Because of the spatially changing energy levels in the modes of interest, the normalized bispectrum, or *bicoherence* was used. In this manner the emphasis was on the *nonlinear phase locking* which is necessary for efficient energy transfer between modes. Finally, to determine the upstream or downstream influence of the flow, the *cross*-bicoherence was calculated for the simultaneously sampled, spatially separated

time series. These consisted of velocity fluctuations in the shear layer at different x-locations along a similarity line, and unsteady pressures at lip at the same azimuthal location. Primary emphasis was placed on the interactions of the fundamental axisymmetric and subharmonic modes in order to document the upstream influence resulting from feedback, their cooperative evolution, and the downstream feedback of those quantities which might have a bearing on the subharmonic resonance and pairing processes.

5.1. *Cross-bicoherence*

The cross-bicoherence (CBC) is a measure of the nonlinear phase locking between frequencies in three time series. The origins of this statistical quantity are given in Appendix B. Its definition is contained in equation (B 14), although the computationally simpler form in (B 17) was used in this study. The time series used in the application of this statistic were the streamwise velocity fluctuations acquired at different spatial locations in jet shear layer, $u(x, r, t)$, and the simultaneous pressure fluctuations at the lip of the jet, $p(t)$ (see figure 1). The third time series is formed by the sum or difference of these two.

When interpreting the CBC estimates, one finds that the order of the interacting frequencies is an important parameter for determining the direction of influence. For two separate time series, such as are used in these studies, as many as nine (three to the power of two) combination orders are possible, although only six are unique. If, for example, a high CBC is observed between frequencies f_1 and f_2 ($f_1 = \omega_1/2\pi$) and their sum or difference frequencies in the time series, three possible interactions could have taken place; namely, that the sum or difference frequencies resulted from the interaction between f_1 and f_2, or f_1 had interacted with the sum or difference frequency to produce f_2, or that f_2 had interacted with the sum or difference frequency to produce f_1. When the origin of a mode frequency is clear, for example if it results from an instability process, this may not be a problem. In the jet, however, because of feedback, it is not always clear whether the pressure field at the lip of the jet originates the velocity fluctuations in the shear layer, or if the velocity fluctuations originate the unsteady pressure field at the lip. To clarify this problem, it becomes necessary to look at the streamwise evolution of the CBC while changing the order of processing of spatially separated time series.

The upper frequency limit of the CBC is set by the Nyquist criterion, such that the sum of any two frequencies cannot exceed half the sampling frequency. From this frequency limit, the region of validity of a coherence plot *for summed interactions* takes the form of a right triangle bounded by a $-45°$ line, crossing the two Cartesian axes at the half-sampling frequency value. The magnitude of the cross-bicoherence is drawn as constant-level contours. By our convention, the processing order of frequencies is such that the first frequency is read from the abscissa, the second one from the ordinate, and the third from the point of intersection between the $-45°$ line and either of the two axes.

Of the six possible independent processing orders, only three were found to be useful. The order of the processing of the CBC greatly affects the result and is therefore indicated on each plot by subscripts: p indicating that it was derived from the pressure signal, and u from the velocity signal. The magnitude of the CBC is plotted as contour levels, starting with the lowest level of 10% and increased by 25% up to 85%. Above each CBC estimate appears the power spectra of the velocity and pressure signals, plotted as solid and dashed lines, respectively. These are plotted with an arbitrarily shifted origin and with a full dynamic range of 50 dB. The pressure spectrum is plotted only for reference and it does not differ from one figure

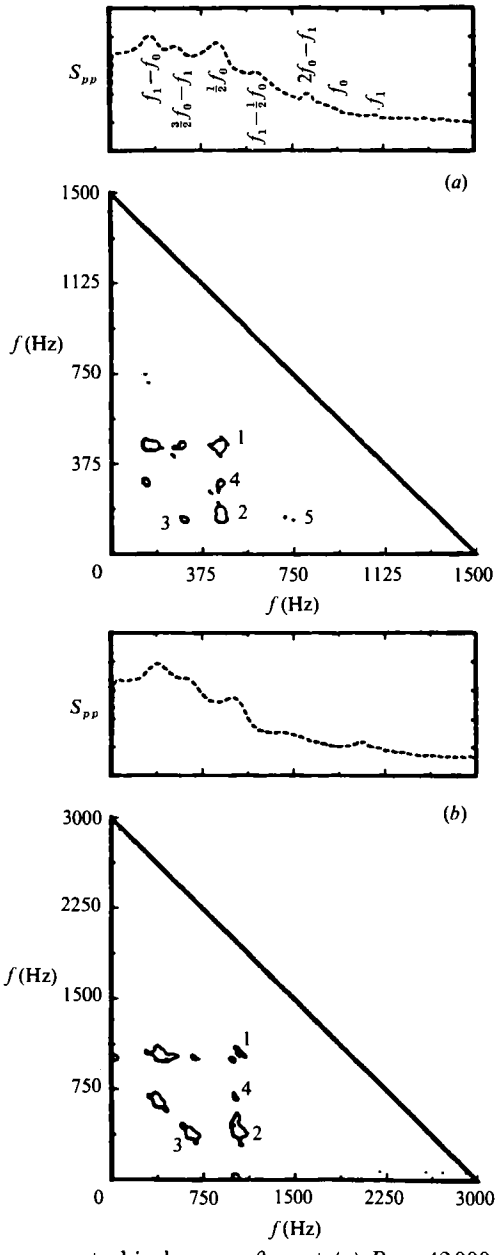

FIGURE 33. Pressure auto-bicoherence β_{ppp} at (*a*) $Re = 42000$ and (*b*) 70000 (1L case, $U/U_j = 0.6$).

to another within the same condition. Also included is the linear coherence between the velocity and the pressure signals. This is plotted as a dotted line, and by definition it falls between zero and one.

5.2. *Nonlinear phase locking for natural jet modes*

The initial phase-locking between the modes measured in the unsteady pressure field at the lip of the jet at both Re = 42000 and 70000 1L cases, is depicted in the auto-bicoherence, β_{ppp}, shown in figure 33. This symmetrical bicoherence exhibits five

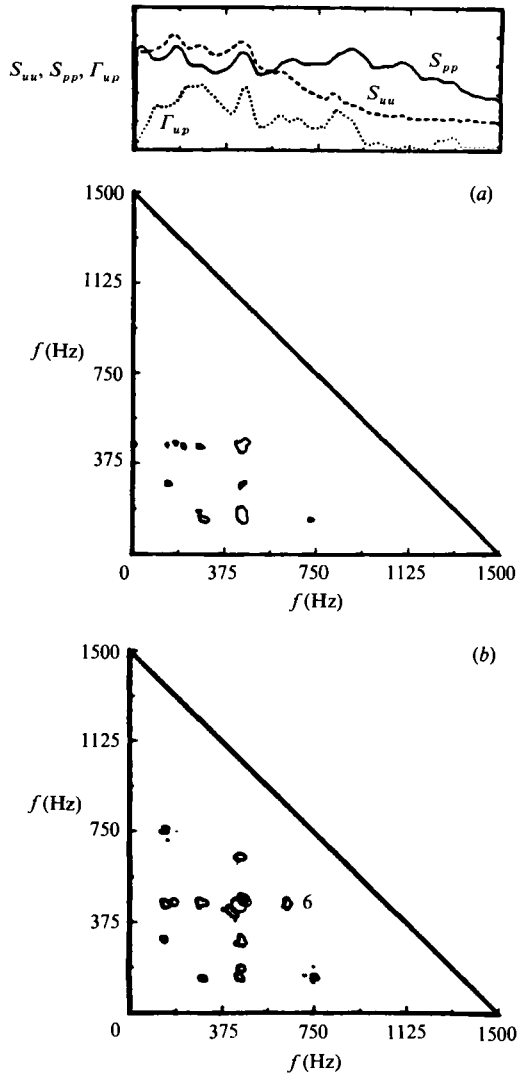

FIGURE 34. (*a*) Velocity–pressure–pressure β_{upp} and (*b*) pressure–pressure–velocity β_{ppu} cross-bicoherence at $x/D = 0.25$ ($Re = 42000$, Case 1L, $U/U_j = 0.6$).

distinguishable peaks, labelled on the figure, which are the result of the interactions between the longer-wavelength modes $\frac{1}{2}f_0$ and $f_1 - f_0$. Peak number 1 signifies the phase locking between the fundamental axisymmetric and subharmonic modes in the triple form $\frac{1}{2}f_0 + \frac{1}{2}f_0 = f_0$. This interaction is stronger in the lower-Reynolds-number case where the initial and final Strouhal numbers are an integer power of two apart. Peak numbers 2 and 3 result from the interaction of the subharmonic mode and the difference mode to produce their sum and difference modes, namely, $\frac{1}{2}f_0 + f_1 - f_0 = f_1 - \frac{1}{2}f_0$ and $\frac{1}{2}f_0 - f_1 - f_0 = \frac{3}{2}f_0 - f_1$. Peak number 4 results from the interaction of the subharmonic mode with the multiple interacted mode of frequency $\frac{3}{2}f_0 - f_1$ to give their sum at frequency $\frac{5}{2}f_0 - f_1$. Peak 5 results from an interaction of the fundamental axisymmetric mode and the interacted mode $f_1 - f_0$ to give the mode at frequency $2f_0 - f_1$. The nonlinear interactions depicted by the auto-bicoherence distributions in

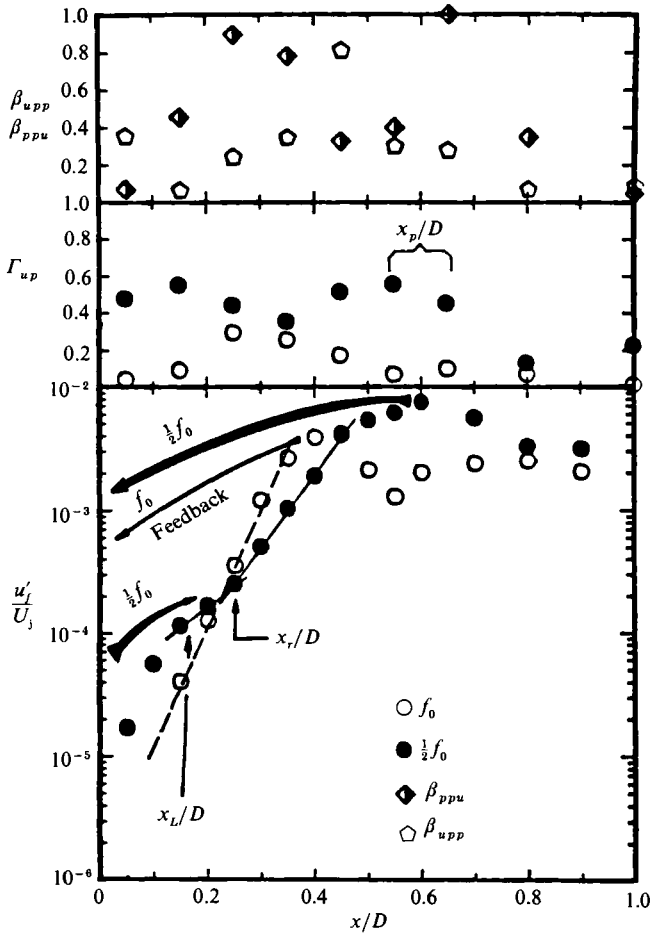

FIGURE 35. Streamwise development of amplitude, coherence, and cross-bicoherence of initial axisymmetric mode and its subharmonic ($Re = 42000$, 1L case, $U/U_j = 0.6$).

this figure represents the initial self-forced 'imprint' resulting from the downstream influence of growing instability and interacted modes in these jets.

In documenting the downstream evolution of the CBC, emphasis will be placed on the interactions involving only the fundamental axisymmetric and subharmonic modes, peak 1 in figure 33. The natural behaviour of the jet at $Re = 42000$ will first be used to point out the essential mechanisms involved in fundamental–subharmonic resonance and feedback. This case will then be used to aid in interpreting the results in jets having different initial disturbance conditions.

A sampling of the cross-bicoherence distributions, β_{ppu} and β_{upp} for the $Re = 42000$, 1L jet is shown in figure 34. This was taken at $x/D = 0.25$, which corresponds to the point where resonant subharmonic growth begins. A composite of results from similar figures taken at different x/D-locations is presented in figure 35 in order to document the fundamental/subharmonic interaction in this jet. This figure includes the streamwise development of β_{ppu} and β_{upp} *for peak 1*, of the linear coherence, Γ_{up}, and of the streamwise velocity fluctuations at f_0 and $\frac{1}{2}f_0$ (reproduced from figure 7).

At the closest measurement location, $x/D = 0.05$ in figure 35, the linear coherence of the subharmonic mode is approximately 50% whereas for the fundamental it is

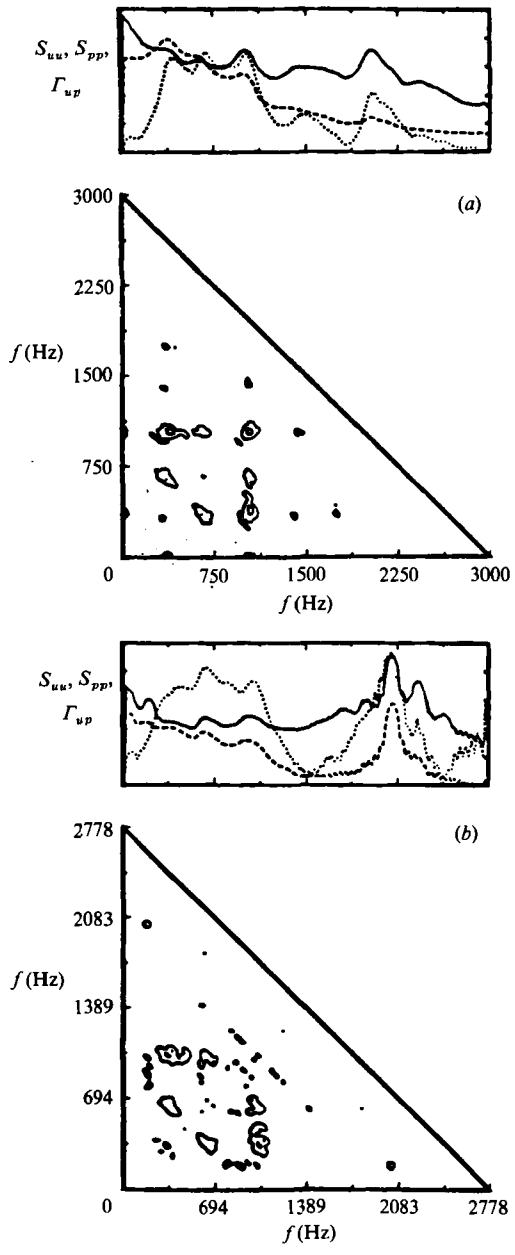

FIGURE 36. Pressure–pressure–velocity cross-bicoherence at $Re = 70000$, $x/D = 0.15$ (case 1L, $U/U_j = 0.6$), for (*a*) unforced jet at 2040 Hz and (*b*) jet forced at 2050 Hz.

almost zero. The small peak of approximately 40% in β_{upp} and the lack of a peak in β_{ppu} indicate that the subharmonic mode at this location is phase locked to the pressure field at the lip, and that no such phase locking is present for the fundamental mode. The relative difference between the magnitudes of β_{upp} and the linear coherence, Γ_{up}, at the subharmonic frequency indicate that the subharmonic mode velocity fluctuations at this most upstream position are linearly phase locked to the pressure fluctuations at the lip.

At $x/D = 0.15$, the linear coherence of both modes has increased slightly. The

cross-bicoherence magnitudes has also increased to a value approximately the same as for the linear coherence. This indicates the beginning of nonlinear interaction between f_0 and $\frac{1}{2}f_0$. By the next location, at $x/D = 0.25$, an abrupt increase in the growth rate of energy at $\frac{1}{2}f_0$ marks the beginning of subharmonic resonance. β_{ppu} at this location is approximately 90% which, when accompanied by the respectively low β_{upp} of approximately 20%, indicates a nonlinear phase locking between f_0 in the velocity field and $\frac{1}{2}f_0$ in the pressure field at the lip. The arrow pointing downstream in the growth curve in this figure signifies this upstream influence of the lip on the subharmonic mode leading to subharmonic resonance.

At $x/D = 0.45$, β_{upp} is now larger than β_{ppu}, suggesting a nonlinear phase locking between $\frac{1}{2}f_0$ in the velocity with f_0 in the pressure. At this same location, the energy at f_0 has reached a maximum. We associate this with the first roll-up of the shear layer into discreet vortices spaced at the fundamental wavelength. The larger β_{upp} suggests that this energetic process results in feedback of fundamental mode energy from the velocity field to the pressure field at the lip. This downstream influence is indicated by the upstream-facing arrow at the frequency f_0. It is drawn lightly to signify that fluctuations at f_0 are only weakly felt at the lip.

At $x/D = 0.65$, β_{ppu} is approximately 100% and significantly larger than β_{upp}. At this location, the energy at $\frac{1}{2}f_0$ has now reached a maximum. This is associated with the approximate point where the formed vortices pair. This indicates that this energetic process results in a nonlinear phase locking between the fundamental mode in the velocity and the subharmonic mode in the pressure. This near-perfect phase locking is strong evidence of feedback of subharmonic mode energy from the velocity field to the pressure field at the lip. This downstream influence is drawn as a bold arrow to signify that it is strongly felt at the lip.

5.3. *Effect of initial disturbances on nonlinear development*

The effect of forcing the $Re = 70000$, 1L jet is summarized in figure 36–38 at the fundamentally important x/D-locations corresponding to the beginning of subharmonic resonance, at the point of fundamental mode energy saturation and at the point of subharmonic mode energy saturations. At the first location at $x/D = 0.15$ in figure 36, the cross-bicoherence β_{ppu} shows a value at peak 1 indicative of the fundamental–subharmonic interaction resulting from the upstream influence of the lip, seen previously at the lower Reynolds number. At the bottom part of the figure, when the jet was forced at f_0, we observe that this peak is not present. This suggests that under the conditions of this mild harmonic forcing, the natural initial nonlinear phase coupling between the fundamental and subharmonic modes has been impeded.

At $x/D = 0.32$ in figure 37, the high peak 1 in β_{upp} in the unforced jet indicates the feedback of energy at the fundamental mode frequency to the lip, again consistent with the lower-Reynolds-number case. The broad diagonal shape of this peak for the jet forced at f_0, however, suggests that the frequency fed back to the lip in this case is phase locked to a broad range of near-subharmonic frequencies. Such interactions would produce the broad peak in the autospectrum at the subharmonic frequency seen at this x/D in this case. Also observed in the autospectra are the discreet sideband modes to the fundamental in the foreed case. The interaction to produce these is seen by the three peaks in β_{upp} centred at the fundamental frequency on the CBC abscissa and aligned to the ordinate frequency of approximately 160 Hz. The 160 Hz frequency may be fundamentally important since it corresponds to a Strouhal number, $fD/U_j = 0.4$, which is the value generally associated with the jet column mode (Ho & Huerre 1984).

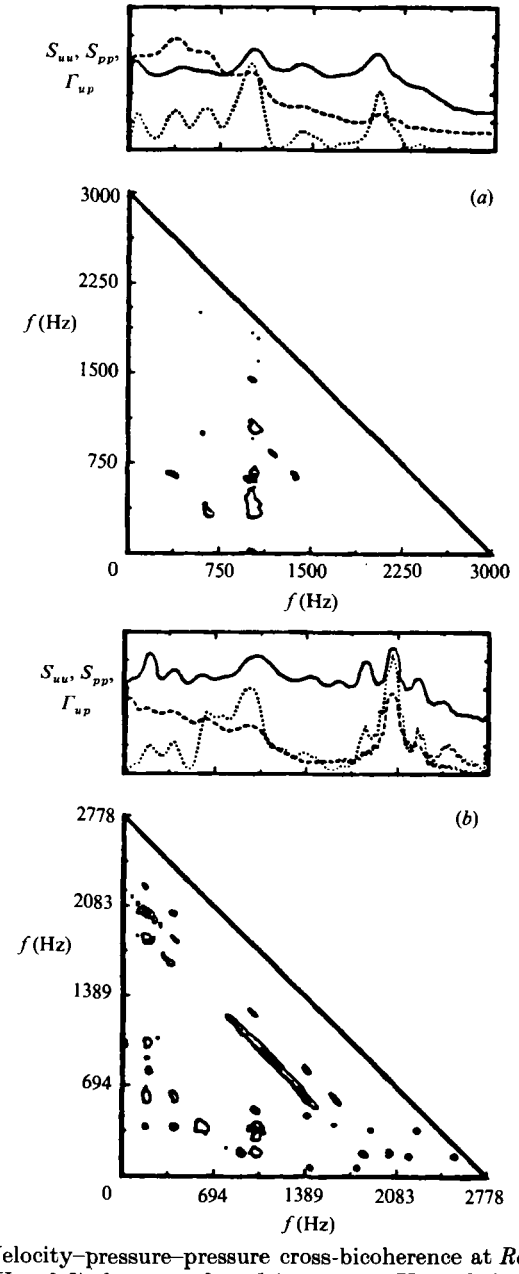

FIGURE 37. Velocity–pressure–pressure cross-bicoherence at $Re = 70000$, $x/D = 0.35$ (case 1L, $U/U_j = 0.6$), for (*a*) unforced jet at 2040 Hz and (*b*) jet forced at 2050 Hz.

By $x/D = 0.45$ in figure 38, the high value of peak 1 in β_{ppu} in the forced jet indicates that the fundamental and subharmonic modes have achieved a concentrated phase locking, comparable with the unforced jet. This subharmonic is fed back and strongly felt at the lip. There also remains some weak nonlinear coupling associated with the fundamental mode sidebands.

The effect of forcing the jet at a frequency 25% higher than the natural f_0 is depicted in figure 39. This shown in figure 39 (*a*) at the x-position of the beginning of

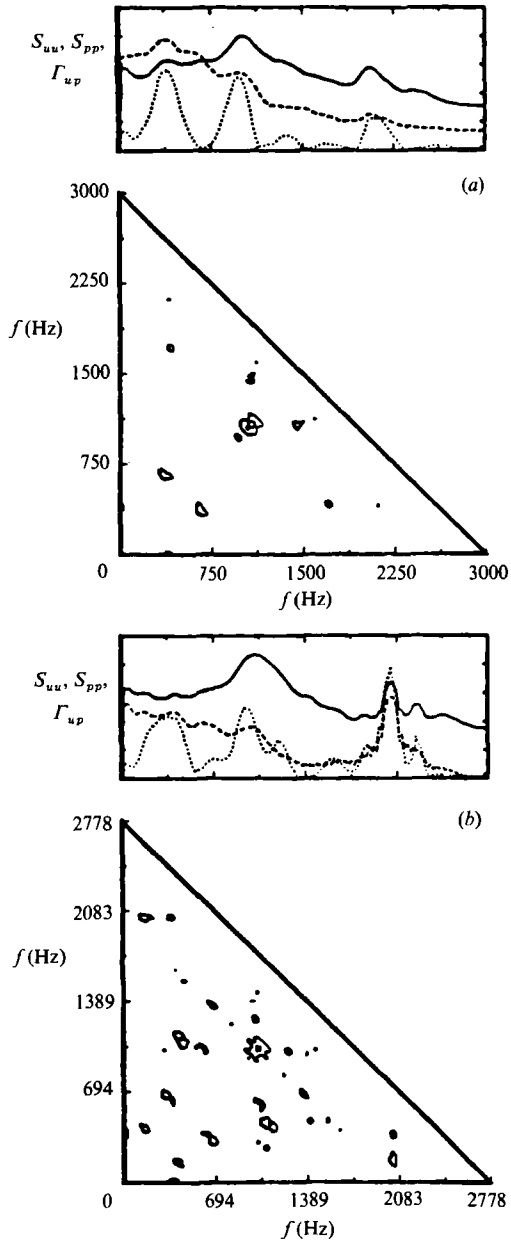

FIGURE 38. Pressure–pressure–velocity cross-bicoherence at $Re = 70000$, $x/D = 0.45$ (case 1L, $U/U_j = 0.6$), for (*a*) unforced jet at 2040 Hz and (*b*) jet forced at 2050 Hz.

enhanced growth of the $\frac{5}{11}f_0$ mode which was seen in figure 18. In this case, we now observe a high organization of the jet with strongly coherent nonlinear interactions. Although the linear coherence of the instability modes for the jet forced at f_0 is comparable, cross-bicoherence levels a factor of two greater exist for this 2500 Hz forced condition, demonstrating a much stronger nonlinear phase locking of these modes in this instance. The interactions involving the $\frac{5}{11}f_0$ mode are apparent in this figure as the band of contour lines at the frequency of 1136 Hz. The source of the non-exact subharmonic is probably a result of the feedback mechanism which acts to

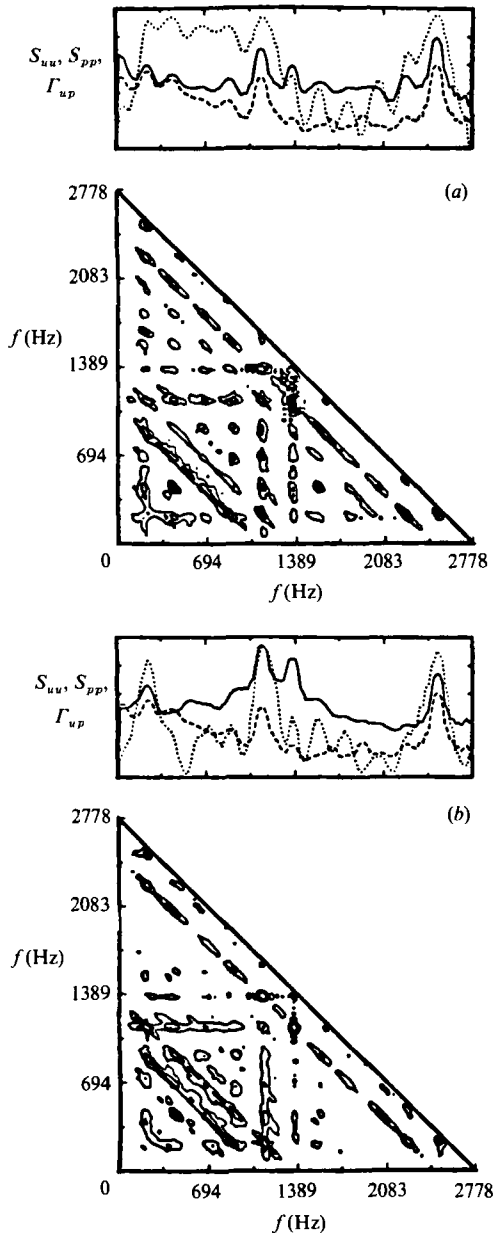

FIGURE 39. Velocity–pressure–pressure cross-bicoherence at (*a*) $x/D = 0.14$ and (*b*) pressure–pressure–velocity cross-bicoherence at $x/D = 0.26$ for jet forced at 2500 Hz at $Re = 70000$ (case 1L, $U/U_j = 0.6$).

select the closest subharmonic frequency which also gives an integer number of wavelengths over the distance from the point of pairing back to the jet lip. This mode interacts with a multitude of other modes to transfer energy to both higher and lower frequencies in discreet fashion to fill the spectrum. The $\frac{1}{11}f_0$ mode, although being close to, is distinguishable from the 160 Hz mode seen in the previous forced case.

Further downstream near the location of energy saturation of the $\frac{5}{11}f_0$ mode, the strong nonlinear phase locking persists. This can be seen in the β_{ppu} distribution in

figure 39 (*b*). At this location, the linear coherence, Γ_{up}, of the forced f_0 and interacted $\frac{5}{11}f_0$ and $\frac{1}{11}f_0$ modes are also still quite high. The large value of β_{ppu} at the frequency intersection of $\frac{5}{11}f_0$ and $\frac{1}{11}f_0$ in the pressure signals suggests that the $\frac{6}{11}f_0$ mode in the velocity fluctuations is a product of that summed interaction. This is also consistent with the insignificant level of the linear coherence at the $\frac{6}{11}f_0$ frequency.

6. Discussion

6.1. *Pairing process and feedback*

In the initial region of the jet shear layer, up to four wavelengths of the fundamental mode, the axisymmetric and subharmonic modes grow exponentially in amplitude, evolve, and interact, leading to the formation of vortical structures and finally pairing. Vortex formation and pairing were observed to result in relatively rapid changes in the streamwise growth of the shear layer, and to provide effective sites for downstream influence of the flow on the unsteady pressure field at the jet exit lip.

At the lip of the jet, a degree of nonlinear phase locking between the fundamental axisymmetric and subharmonic modes was found to exist initially. This was seen from the auto-biocoherence distribution in figure 33. Nonlinear phase locking also existed between other frequencies in the pressure field at the lip as a result of sum and difference interactions with the longer-wavelength $\frac{1}{2}f_0$ and (f_1-f_0) modes. These represented a natural tuned self-forced condition of the initial shear-layer growth.

Within the first approximately two fundamental wavelengths downstream of the jet exit, the fundamental and subharmonic modes grow independently. Their initial amplitudes are commensurate with the degree of tuned self-forcing as well as other competing background disturbances. Evidence of their independent growth comes from the difference in their phase velocities (figure 10), which makes energy transfer inefficient. The lack of intercomponent mode locking was evident in the low levels of cross-bicoherence in this early region at the top of figure 35.

In this early stage, the fundamental mode is best characterized by a wave representation with a double-peaked eigenfunction modulus. The fluctuation minimum between these corresponded to the location of a 180° phase shift in the eigenfunction phase. Prior to vortex formation, there existed virtually no growth in the momentum thickness downstream, and the mean profile closely followed a hyperbolic tangent distribution. When these characteristics are combined, one can see the origin of agreement to analysis with linear, spatial, inviscid, parallel stability theory.

At the end of this region (two fundamental wavelengths from the jet exit), the secondary enhanced growth of the subharmonic begins. This was marked by a reduction of the phase velocity of the subharmonic to match that of the fundamental. This change was seen as the rapid shift in the subharmonic eigenfunction phase at $x/D = 0.3$ in figure 6, requiring less than a quarter of a subharmonic wavelength to make the transition.

In the process of changing phase velocities, the linear coherence, Γ_{up}, is low. This would be expected since this statistic is a measure of linear phase locking and the subharmonic phase development is changing at this location. In contrast to this, the high cross-bicoherence, β_{ppu}, for a fundamental/subharmonic interaction indicates a strong degree of nonlinear phase locking between these modes. When combined with the lower β_{upp} at this location this documents phase locking between the subharmonic in the pressure field at the lip, and the fundamental in the velocity field at this x/D. We interpret this as the upstream influence of the pressure field at the

lip to aid in adjusting the phase velocity of the subharmonic mode, satisfying the resonance condition and leading to its enhanced growth.

The region of influence of the lip is fairly localized, and does not extend far downstream of this point. This was evident from the decreasing β_{ppu} and increasing β_{upp} past $x/D = 0.3$ in figure 35, prior to fundamental mode saturation.

Fundamental mode saturation occurs one wavelength downstream of this point (three wavelengths from the jet exit). This process is associated with the first roll-up of the shear layer into a vortex ring. The high β_{upp} for a fundamental/subharmonic interaction indicates the strong degree of nonlinear phase locking between these modes which is associated with this event. The direction of the interaction is inferred from the simultaneously low β_{ppu}. These indicate a nonlinear phase locking between the subharmonic in the velocity, and the fundamental in the pressure (at the lip). We interpret this to result from feedback of pure-tone acoustic disturbances at the fundamental frequency from the point of vortex roll-up back to the jet lip. This feedback was indicated by the light arrow in figure 35. The energy in pressure fluctuations at the fundamental frequency at the lip is however relatively small, suggesting that the downstream influence of this mode is weak.

The subharmonic mode continues to grow exponentially for another fundamental wavelength downstream of the point for fundamental mode saturation, four wavelengths from the lip. Since the beginning of its secondary growth, its growth rate was close to that of the fundamental. When the subharmonic mode saturates, a nearly perfect nonlinear phase locking existed for the β_{ppu} fundamental/subharmonic interaction. When combined with the relatively low β_{upp}, this indicated that the phase locking occurred between the fundamental in the velocity and the subharmonic in the pressure (at the lip). We interpret this to result from acoustic feedback at the subharmonic frequency produced by the energetic process of vortex pairing which is associated with this energy maximum. This process was indicated by the bold arrow pointing in the upstream direction in figure 35. A larger, dominant peak in the pressure spectrum at the subharmonic frequency indicates that the downstream influence of this mode is relatively strong. The dominance of this mode is similarly seen in the spectral-peak historgram of MEM spectral estimates in figures 24 and 26. The influence is especially strong in the 42000 Reynolds number jet for which the final frequency coupling existed. However, the importance of subharmonic mode feedback is not restricted to only this extra special condition.

6.2. *Non-axisymmetric modes*

Analysis by Michalke (1971) and Mattingly & Chang (1974) had indicated that the initial region of the jet is equally unstable to both axisymmetric and non-axisymmetric (helical) modes. In a previous experiment using the same facility as in this investigation, Drubka (1981) had documented the $m = \pm 1$ helical mode in addition to the fundamental axisymmetric modes. Although his observations were based on long-time-averaged spectral estimates, he speculated that the initial region alternates between these fundamental states. In the present experiment, long-time-averaged spectra brought out the existence of these two modes. The streamwise frequency of these and the dependence on Reynolds number was found to be in agreement with Drubka's values. To answer Drubka's speculation, short-time mode analysis was performed using maximum entropy spectral estimates in order to observe their temporal behaviour.

Mode detection was based on the existence of spectral peaks in the short-time estimates at the frequencies for the fundamental axisymmetric and $m = \pm 1$ helical

modes, respectively. The temporal evolution of these modes was seen in a qualitative sense in figures 21 and 22 for the natural jets. These indicated a lack of coexistence and apparent non-deterministic switching between fundamental states. This was quantified in spectral-peak occurrence distributions of the type shown in figures 30 and 31 and in the cross-occurrence distributions in figure 32.

The spatial exponential growth rate of the helical mode was found to be the same as that of the axisymmetric mode, in agreement with theory. The average initial amplitudes close to the jet exit were also very similar. In addition, their streamwise extent of constant exponential growth was found to be quite comparable so that their points of energy saturation coincided closely. Presumably then, the dominant mode at any instant is likely to be the one that had the highest initial amplitude forcing due to randomly arriving axisymmetric or non-axisymmetric disturbances at the jet lip. When the jet was disturbed by far-field harmonic acoustic disturbances which excite axisymmetric modes, the existence of the helical mode was effectively suppressed. In the case of non-axisymmetric modes, a disturbance which produces a 180° azimuthal phase difference around the exit lip would be suitable to produce a $m \pm 1$ helical mode.

One might expect that the percentage of occurrence of each of these fundamental modes would have a constant value throughout the jet initial region. The spectral peak occurrence distributions in figures 30 and 31 show that this is in fact not the case. This suggests that these modes can overtake and suppress each other through interactions further downstream. For example, the occurrence of the helical mode was observed to reach its maximum at the x/D-location associated with the beginning of subharmonic resonance. At this location, the occurrence of the subharmonic is a minimum.

The percentage of time that both the fundamental axisymmetric and helical modes coexist was found to be negligibly small. The only exception was at the beginning of subharmonic resonance where their simultaneous occurrence reached approximately 4%. It was only in this region that the cross-bicoherence showed a nonlinear phase locking between the axisymmetric subharmonic and helical modes to produce the difference mode $f_1 - \frac{1}{2}f_0$. The otherwise general anti-correlation between the occurrence of these two fundamental modes suggests that each might be a basin of attraction which suppresses the existence of the other.

Given this physical picture for the alternate existence of these two fundamental modes, we are left in somewhat of a quandary as to the origin of the difference mode, $f_1 - f_0$. That is, how could these two modes interact to produce their difference mode if they do not coexist?

We have observed the existence of this mode in the pressure and velocity time series. Along with the subharmonic mode, it dominates the lip-pressure field to produce a number of nonlinearily phase-locked modes formed from sum and difference interactions, which provide a level of initial jet self-forcing. The spatial amplification of the $f_1 - f_0$ mode exhibits two constant exponential growth regions, similar to the subharmonic. The x/D-location of the change in exponential growth is at the same point as that of subharmonic. Also, their spatial growth rates are nearly the same. Since the difference frequency is far from the region of maximum linear amplification, this high growth attests to the nonlinear energy transfer to this mode. Since the spatial growth mimics that of the axisymmetric subharmonic, we expect that these two modes are related. If we look to the auto-bicoherence, β_{ppp}, at the lip of the jet in figure 33, peak 2 documents a nonlinear phase locking between the subharmonic and difference mode in the form $\frac{1}{2}f_0 + f_1 - f_0 = f_1 - \frac{1}{2}f_0$. This interacted

mode in the unsteady pressure is observed to interact with the subharmonic in the unsteady pressure in peak 6 of the β_{ppu} in figure 34, to produce nonlinear phase locking with the helical mode at f_1 in the velocity at the beginning of secondary exponential growth. Therefore, we do observe a close link between the f_1-f_0 and $\frac{1}{2}f_0$ modes which originates in the fed-back unsteady pressures at the jet lip and, through the lip influence, had a downstream effect to produce a nonlinear phase locking between $\frac{1}{2}f_0$ and f_1. Recall that the only point of non-zero coexistence of the f_0 and f_1 modes was at the location of the emergence of peak 6 in figure 34, which was also the location of the occurrence maximum of the f_1 mode.

When the jet was excited by far-field acoustic pure tones at the axisymmetric mode frequency, f_0, the helical mode at frequency f_1 is effectively suppressed. But, was it eliminated totally ? Examining figure 31 (*b*) shows some traces of occurrence of the f_1 mode (dotted) which still contain the same x/D trends as in the natural case, shown in the plot above it. Remember that the acoustic excitation was not meant to totally overwhelm the jet but rather to favour certain modes.

The overall occurrence levels of the f_1-f_0 mode had been reduced by the axisymmetric excitation. This is seen both in the pressure field at the jet lip and by comparing the distributions in figures 31 (*a*) and 31 (*b*) (dash-dotted). The reduction is not linearly proportional to the lowering of the f_1 occurrence. However, since the growth of the f_1-f_0 mode is also nonlinearily linked to the $\frac{1}{2}f_0$ mode, which has been shown to be resonantly locked with the f_0 mode, even a trace amount of energy at f_1 could result in a disproportionate energy transfer into the helical mode at the difference frequency. Recall that the occurrence statistics make no distinction between the amplitudes of these modes, only their existence in the time series. In fact, the amplitude of the f_1-f_0 mode, relative to f_0, is significantly less with axisymmetric mode excitation.

6.3. *Effect of initial forcing*

In addition to the pure-tone acoustic excitation at f_0, acoustic forcing away from the natural axisymmetric mode and broadband core disturbances had been imposed to study their effects on the initial development of unstable modes in the jet. In the previous section the effect of axisymmetric mode forcing on the helical modes was discussed. A sensitive and consistent indicator of the x-development of the unstable modes is the mode occurrence distributions such as in figure 31. We therefore look to these to show some of the effects of the weak acoustic excitation. In terms of the axisymmetric modes, the forcing at f_0 gave the expected initial increase in the occurrence of that mode near the lip. The level of occurrence, however, had gradually decreased towards the unforced behaviour by the location of fundamental mode saturation. Recall that the level of forcing was only 0.05% of the dynamic pressure which would be of the same order as the natural feedback levels.

We observe in Figures 31 (*a*) and 31 (*b*) that the forcing at f_0 had altered the occurrence development of the subharmonic mode (solid line). In particular, upstream of the location of the beginning of resonant subharmonic growth ($x/D = 0.25$), the occurrence levels are significantly lower for that mode. In the region of secondary growth, the occurrence of the subharmonic increases at a slower rate and reaches a maximum further downstream. Since this maximum is associated with vortex pairing, the low-amplitude forcing at f_0 appears to have slightly retarded this process.

To understand this effect better, we look at the fundamental/subharmonic interactions brought out by the CBC in figures 36–38. Recall that the x/D-locations

for these three figures corresponded to the fundamentally important positions: the beginning of subharmonic resonance aided by the upstream influence of the unsteady pressures at the lip; the saturation of the fundamental mode which provides weak feedback at f_0 to the lip; and the saturation of the subharmonic mode which provides strong feedback at $\frac{1}{2}f_0$ to the lip. By interpreting these figures, the low-amplitude forcing at f_0 had diminished the upstream influence of the lip by decoupling the nonlinear phase locking between the f_0 and $\frac{1}{2}f_0$ modes. In essence, in this initial region there are two frequency sources feeding the unsteady pressure field at the lip. The first is due to the acoustic input from a sine generator and speaker. The second is due to the response of the jet and the closed-loop feedback at $\frac{1}{2}f_0$. These two frequencies, being derived from separate sources, are therefore not phase locked.

We can observe some subtle effects of the lack of initial phase locking of these two modes, for example in the beginning of secondary subharmonic growth in figure 16. Generally, we have observed a sharp change in subharmonic growth which was accompanied by a rapid change of phase velocity of the subharmonic to match that of the fundamental. With the mild forcing at f_0, we observe a much more gradual change in growth of $\frac{1}{2}f_0$, which is also delayed relative to the downstream development of the fundamental. This can also be traced to a reduction in the local spreading rate of the jet between $x/D = 0.35$ and 0.45 in figure 11, which is in the region of secondary subharmonic growth. Past the point of pairing, the spreading rate of the jet forced at f_0 has overcome this early reduction and slightly surpasses that of the natural jet. This behaviour might be due to the observed additional nonlinear phase locking with the column mode (160 Hz) that appeared only in this specific forced case.

A recent paper by Monkewitz (1988) predicts subharmonic resonance on the basis of the fundamental mode achieving a minimum amplitude, $u'_f/U_j = 0.015$. Based on this, we can compare the amplitudes of the fundamental axisymmetric modes at the x-position of first enhanced subharmonic growth (x_r/D) for the different cases examined here. In the unforced jet, 1L condition, at both Reynolds numbers, the maximum streamwise velocity fluctuation levels seen from figures 8 and 14 was roughly the same and equal to 0.0003. This of course is considerably below that predicted by Monkewitz, but in experiments the absolute levels are somewhat ambiguous since they vary with the spectral bandwidth. For example, Monkewitz's good agreement to Drubka's $Re = 42000$ data is two orders of magnitude off when the amplitudes are converted to the standard 1 Hz bandwidth, as we had done in the comparison in figure 7.

Therefore, rather than compare absolute levels, we can examine effects of different initial conditions, most notably between unforced and forced jets. Specifically, this involves our jet at $Re = 70000$, with the spatial growth curves seen in figures 14 and 16. In this comparison, for the forced jet, we observe an almost order of magnitude increase in the threshold level of the fundamental mode at the x-position of secondary subharmonic growth. Since we have interpreted the effect of our mild forcing as disrupting the natural feedback mechanism and delaying subharmonic resonance, this result seems to support that mechanism over one strictly based on amplitude alone.

Forcing the jet at a frequency 25% higher than the natural selected f_0 resulted in a more strongly organized jet with strong feedback at $\frac{1}{11}f_0$ and $\frac{5}{11}f_0$ frequencies. The initially shorter-wavelength fundamental frequency and strong resonant interaction with the $\frac{5}{11}f_0$ mode resulted in faster spreading in this case.

The non-exact $\frac{5}{11}f_0$ 'subharmonic' in this case was probably selected by the flow in

order to satisfy a constraint imposed by feedback that there be an integer number of wavelengths from the feedback source, in this case the x/D of pairing, back to the lip of the jet. This selection resulted in a much stronger nonlinear phase locking and a high degree of organization of a broad band of discreet sum and difference modes that was not apparent with weak harmonic forcing. This exercise demonstrates an efficient means of control of the early jet instabilities by making use of the natural upstream influence of the lip and the downstream influence of related modes which are associated with the energetic motions of vortex formation and successive pairings.

Observations such as resonant mode selection and harmonic spectra indicate that a convectively unstable flow (a cold axisymmetric jet) in the presence of feedback appears to share some of the features related to absolutely unstable flows. Such a distinction has profound implications with respect to the possible existence of deterministic chaos in jets as well as issues of flow controllability.

7. Conclusions

The results have documented the existence and exponential growth of the two fundamental modes in the axisymmetric jet shear layer, namely the axisymmetric and $m = \pm 1$ helical modes. In the case of the former, a parametric interaction between it and its subharmonic was found to exist and to be an important factor in the early development of the jet. This interaction was marked by a matching of their phase velocities, requiring a decrease in the phase velocity of the subharmonic, the resonant exchange of energy from the fundamental mode to the subharmonic, and a resulting enhanced exponential growth of the subharmonic mode leading to large amplitudes and eventual energy saturation. A key factor of this process was the recursive feedback of energy from the sites of the first vortex rollup and vortex pairing. These acted to produce a self-forced phase locking of the initial fundamental and subharmonic modes which later led to the early resonant growth of the subharmonic mode, within two fundamental axisymmetric wavelengths. This resonant feedback mechanism gives the jet some of the features attributed to absolutely unstable flows, which may have profound implications for their controllability.

Underlying the resonant organization seen in the axisymmetric modes was the development and growth of the $m = \pm 1$ helical modes. Short-time spectral estimates were used to document the temporal evolution of the helical and axisymmetric modes. These indicated a lack of coexistence and apparent non-deterministic switching between these two fundamental states. At any time, the dominant mode was likely to be the one with the higher initial forcing level due to randomly arriving axisymmetric or non-axisymmetric disturbances at the jet lip. With this scenario in mind, a low-dimensional temporal model based on the competition between these two modes may be useful to capture the early random nature which we attributed to spectral broadening at these mode frequencies in the initial jet exit region.

This work has been supported by grants from the US Air Force Office of Scientific Research, particularly F49620-80-C-0053 which was monitored by Major Michael Francis, and F49620-86-C-0165 which is monitored by Dr James McMichael.

Appendix A. Maximum entropy spectral estimates

Recently, spectral estimations based on the maximum entropy method (MEM) have been adopted at IIT for the analysis of data series from unsteady fluid dynamics experiments. The main feature of this method is that it allows the determination of spectra for exceedingly short time series where methods based on DFT fail to produce accurate results. Extensive documentation of the characteristics and usage of this method has been done by us on time series derived in this and other fluid flows. The following discussion is meant to provide an overview of the theoretical basis for the method and to document its use in this study.

The maximum entropy time series is determined to be the one in which the entropy, $E(S)$, of the power spectrum, $S(\omega)$, defined as

$$E(S) = \int_{-\omega_n}^{\omega_n} \log S(\omega)\, \mathrm{d}\omega, \tag{A 1}$$

is a maximum, under the constraint that the spectrum also be consistent with the first $M+1$ measured lags of the auto-correlation function, R_k. The autocorrelation is defined to be the inverse Fourier transform of the power spectrum, namely

$$R_k = \int_{-\omega_n}^{\omega_n} S(\omega)\, \mathrm{e}^{\mathrm{i}\omega k \Delta t}\, \mathrm{d}\omega \quad (-M \leqslant k \leqslant M). \tag{A 2}$$

Here, Δt is the time increment, k is a discrete time index, ω is the angular frequency, ω_n is the angular Nyquist frequency, and i is the square root of negative one.

Defining the Lagrange multiplier λ_k, the solution for $S(\omega)$ which maximizes this variational problem is

$$S(\omega) = \frac{1}{\sum_{k=-M}^{M} \lambda_k\, \mathrm{e}^{\mathrm{i}\omega k \Delta t}} \tag{A 3}$$

where the λ satisfy the constraint equation (A 2).

The traditional transform notation is obtained by setting

$$z = \mathrm{e}^{\mathrm{i}\omega \Delta t}, \tag{A 4}$$

where

$$S(z) = \ldots + R_{-M} z^{-M} + \ldots + R_0 + \ldots + R_M z^M + \ldots$$

and R_0, R_1, ..., R_M are known $M+1$ auto-correlation coefficients. The power spectrum, $S(\omega)$, is related to $S(z)$ by the z-transform of the auto-correlation function, namely

$$S(z) \langle - \rangle (z = \mathrm{e}^{-\mathrm{i}\omega \Delta t}) \tag{A 5}$$

In factored form,

$$S(z) = \frac{\sigma_M^2}{A_M(z)\, A_M(z^{-1})}, \tag{A 6}$$

where

$$A_M(z) = 1 + a_1 z + \ldots + a_M z^M \tag{A 7}$$

is a $(M+1)$ length prediction-error filter with variance σ_M^2. Expressing (A 6) in the frequency domain and combining it with (A 3), one obtains the MEM spectral estimate

$$S(\omega) = \frac{1}{\sum_{k=-M}^{M} \lambda_k\, \mathrm{e}^{\mathrm{i}\omega k \Delta t}} = \frac{\sigma_M^2}{(A_M(\omega))^2}. \tag{A 8}$$

The right-hand side of the equality in (A 8) can also be found by modelling the time series as an auto-regressive series of order M. Such a model therefore maximizes the entropy in the time series.

The problem that remains is to compute the prediction-error filter coefficients $A_M(\omega)$, and to determine the 'best' order, M, for the auto-regressive model. The approach to the first part is due to Burg (1967) who suggested minimizing the average of the sum of both the mean-square prediction and hindsight errors, P_1, to find the first coefficient a_{11}. For an N-point data series, that quantity is defined as

$$P_1 = \frac{1}{2(N-1)} \sum_{i=1}^{N-1} (x_{i+1} + a_{11}\, x_i)^2 + (x_i + a_{11}\, x_{i+1})^2. \tag{A 9}$$

The remaining coefficients are then found from the Toeplitz recursion formula

$$a_{M,s} = a_{M-1,s} + a_{M,M}\, a_{M-1,M-s}; \quad s = 1, \ldots, M-1. \tag{A 10}$$

The order, M, of the prediction-error filter remains the key parameter in calculating the most appropriate spectrum. Many empirical studies utilizing synthetic data having known spectral content have been conducted in order to develop measures for determining the proper filter length. Reisenthel & Corke (1983) have studied a number of these and identified four regions of behaviour with increasing filter length, M. In the first region, A, with the shortest filter lengths, only a smooth envelope of the distribution having no spectral peaks is obtained. In the next region, B, which starts from the end of the region A, with increased filter length, the spectral peaks that emerge have the correct amplitude and frequency; however, some combining of closely neighbouring peaks may occur at lower frequencies. In region C all of the spectral peaks are identified; however, their amplitudes may not be correct. Finally in region D peak splitting is observed to occur, leading to incorrect spectral estimations.

These criteria were used to determine the proper filter length for the analysis of the data series in this study. In the approach here the method was used to detect the *existence* of the various modes and to follow their spatial and temporal evolution, without interest in their amplitude. Therefore a prediction-error filter length was chosen which placed us within the region C above described. Owing to the nature of the time series, all of the selection criteria had shown a broad C region for all of our flow cases.

Appendix B. Cross-bicoherence

The cross-bicoherence is a measure of the nonlinear phase locking between frequencies in three time series. In a general sense, these time series are represented as $u_1(t)$, $u_2(t)$, and $u_3(t)$. For simplicity these are not shown to be a function of their spatial position. The Fourier transforms of these time series are defined as

$$u_i(t) = \int_{-\infty}^{\infty} \tilde{u}_i(\omega)\, \mathrm{e}^{\mathrm{i}\omega t}\, d\omega; \quad i = 1, 2, 3, \tag{B 1}$$

$$\tilde{u}_i(\omega) = \frac{1}{2\pi} \int_{-\infty}^{\infty} u_i(t)\, \mathrm{e}^{-\mathrm{i}\omega t}\, \mathrm{d}t, \tag{B 2}$$

where $\tilde{}$ denotes the transformed function in the wavenumber domain, ω is the wavenumber, and i is the square root of negative one.

The first three statistical moments of these time series are given as:

the first order,

$$R_i = \langle u_i(t) \rangle; \quad i = 1, 2, 3; \tag{B 3}$$

the second order,

$$R_{ij}(\tau) = \langle u_i(t)\, u_j(t+\tau) \rangle; \quad i, j = 1, 2, 3; \tag{B 4}$$

and the third order,

$$R_{ijk}(\tau_1, \tau_2) = \langle u_i(t)\, u_j(t+\tau_1)\, u_k(t+\tau_2) \rangle; \quad i, j, k = 1, 2, 3, \tag{B 5}$$

where $\langle\rangle$ denotes the realizations ensemble average, and τ is a time delay.

The first-order moment is the mean of the time series. The second-order moment is the correlation. The correlation is a measure of the linear interaction between quantities in the two time series. The correlation can also be determined from the Fourier transform of the times series, namely

$$R_{ij}(\tau) = \frac{1}{2\pi} \int_{-\infty}^{\infty} \langle \tilde{u}_i(\omega)\, \tilde{u}_j^*(\omega) \rangle\, \mathrm{e}^{\mathrm{i}\omega t}\, \mathrm{d}\omega, \tag{B 6}$$

where * denotes the complex conjugate. The product $\langle \tilde{u}_i(\omega)\, \tilde{u}_j^*(\omega) \rangle$ is the cross-spectrum between $u_i(t)$ and $u_j(t)$.

The third-order moment is a measure of the linear and quadratic interaction between the three time series, as seen in (B 5). In order to better appreciate the origin of the bispectrum it is helpful to derive the relation between the third-order moment and the Fourier transform of the time series. The Fourier transform of R_{ijk} is

$$\tilde{R}_{ijk}(\omega_1, \omega_2) = \frac{1}{4\pi^2} \int_{-\infty}^{\infty} \langle u_i(t)\, u_j(t+\tau_1)\, u_k(t+\tau_2) \rangle\, \mathrm{e}^{-\mathrm{i}\omega_1 t_1 - \mathrm{i}\omega_2 t_2}\, \mathrm{d}\tau_1\, \mathrm{d}\tau_2. \tag{B 7}$$

Notice that $\tilde{R}_{ijk}$ is a function of two wavenumbers, ω_1 and ω_2.

In (B 7), replacing the time series by their Fourier integral transform, as defined in (B 2), and interchanging the order of integration and the ensemble average, the following equation can be derived:

$$\tilde{R}_{ijk}(\omega_1, \omega_2) = \frac{1}{4\pi^2} \int_{-\infty}^{\infty} \langle \tilde{u}_i(\omega)\, \tilde{u}_j(\omega')\, \tilde{u}_k(\omega'') \rangle\, \mathrm{e}^{-\mathrm{i}\omega_1 \tau_1 - \mathrm{i}\omega_2 \tau_2} \times \mathrm{e}^{\mathrm{i}\omega t + \mathrm{i}\omega'(t+\tau_1) + \mathrm{i}\omega''(t+\tau_2)}\, \mathrm{d}\omega\, \mathrm{d}\omega'\, \mathrm{d}\omega''\, \mathrm{d}\tau_1\, \mathrm{d}\tau_2. \tag{B 8}$$

By taking advantage of Kronecker delta function relations

$$\frac{1}{2\pi} \int_{-\infty}^{\infty} \mathrm{e}^{\mathrm{i}(\omega_1 - \omega_2)\tau}\, \mathrm{d}\tau = \delta(\omega_1 - \omega') \tag{B 9}$$

and

$$\int_{-\infty}^{\infty} f(\omega')\, \delta(\omega - \omega')\, \mathrm{d}\omega' = f(\omega), \tag{B 10}$$

(B 8) simplifies to

$$\tilde{R}_{ijk}(\omega_1, \omega_2) = \int_{-\infty}^{\infty} \langle \tilde{u}_i(\omega)\, \tilde{u}_j(\omega_1)\, \tilde{u}_k(\omega_2) \rangle\, \mathrm{e}^{\mathrm{i}(\omega + \omega_1 + \omega_2)t}\, \mathrm{d}\omega. \tag{B 11}$$

With the assumption that the series is stationary, rigorous algebra is needed to simplify the above equation. However, in order to avoid these steps, a shorter approach can be adopted. Knowing that the result of the above integral is not a

function of time, which requires $\omega+\omega_1+\omega_2$ to be equal to zero, the following relation is derived:

$$\tilde{R}_{ijk}(\omega_1,\omega_2) = \langle \tilde{u}_i(\omega)\,\tilde{u}_j(\omega_1)\,\tilde{u}(\omega_2)\rangle\,\delta(\omega+\omega_1+\omega_2). \tag{B 12}$$

Defining $\tilde{u}^*(\omega)$ as the complex conjugate of $u(\omega)$, then

$$\tilde{R}_{ijk}(\omega_1,\omega_2) = \langle \tilde{u}_i(\omega_1)\,\tilde{u}_j(\omega_2)\,\tilde{u}_k^*(\omega_1+\omega_2)\rangle. \tag{B 13}$$

The function $\tilde{R}_{ijk}(\omega_1,\omega_2)$ is the cross-bispectrum which will be denoted here as $B_{ijk}(\omega_1,\omega_2)$.

What is the physical interpretation of this quantity? The cross-bispectrum is a measure of the energy transfer resulting from the quadratic interaction of two wavenumbers in two time series to produce their sum or difference wavenumber in a third time series. In the present experiment, which dealt with resonant mode interactions, it was more instructive to measure the level of the nonlinear phase locking rather than the amount of energy transfer. Therefore, the normalized cross-bispectrum, or cross-bicoherence, was utilized.

The cross-bicoherence (CBC) is defined as

$$\beta_{ijk}(\omega_1,\omega_2) = \frac{|B_{ijk}(\omega_1,\omega_2)|^2}{\langle|\tilde{u}_i(\omega_1)|^2\,|\tilde{u}_j(\omega_2)|^2\rangle\,\langle|\tilde{u}_k(\omega_3)|^2\rangle}, \tag{B 14}$$

where i, j, and k refer to the time series with wavenumbers ω_1, ω_2, and ω_3, respectively, and $|\cdot|$ is the modulus of the component. These wavenumbers are related to each other such that $\omega_1+\omega_2+\omega_3=0$. In the experiment in the jet, the time series were the streamwise velocity fluctuations, acquired at different spatial locations in the shear layer, $u(x, r, t)$, and the simultaneous pressure fluctuations at the lip of the jet, $p(r, t)$. The subscripts i, j and k refer to these two measured time series. For the case when i, j, and k are the same, $\beta_{ijk}(\omega_1,\omega_2)$ will be symmetric with respect to ω_1 and ω_2, and will be referred to as the auto-bicoherence (ABC).

In the above equation, the calculation of the quantity

$$\langle|\tilde{u}_1(\omega_1)|^2\,|\tilde{u}_j(\omega_2)|^2\rangle \tag{B 15}$$

requires considerable computer time and memory storage for respectably sized transforms. Therefore, it is convenient to replace it by the quantity

$$\langle|\tilde{u}_i(\omega_1)|^2\rangle\,\langle|\tilde{u}_j(\omega_2)|^2\rangle. \tag{B 16}$$

To justify this substitution, several tests had been conducted on synthetic data having a known cross-bicoherence. In order to simulate the types of time series we could expect from this experiment various levels of random noise were also superposed on the tested time series. It was found that for a large enough number of realization averages, the difference between these two quantities was small. Therefore making this simplification, the final form of the cross-bicoherence used was

$$\beta_{ijk}(\omega_1,\omega_2 = \frac{|B_{ijk}(\omega_1,\omega_2)|^2}{\langle|\tilde{u}_i(\omega_1)|^2\rangle\,\langle|\tilde{u}_j(\omega_2)|^2\rangle\,\langle|\tilde{u}_k(\omega_3)|^2\rangle}. \tag{B 17}$$

From the Schwarz inequality, the cross-bicoherence falls between the values of zero and one. When, from realization to realization the degree of triple phase locking

$$\theta_i(\omega_1)+\theta_j(\omega_2)-\theta_k(\omega_3) \tag{B 18}$$

is high, the CBC will have a value close to one. Here $\theta_i(\omega_1)$ is the instantaneous circular phase angle of $\tilde{u}_i(\omega_1)$. The maximum level of the CBC estimate is however

dependent on the signal-to-noise ratio of the data series. When no phase locking exists it is of zero.

REFERENCES

ACTON, E. 1980 A modelling of large eddies in an axisymmetric jet. *J. Fluid Mech.* **98**, 1–31.

BROWAND, F. K. & LAUFER, J. 1975 The role of large scale structures in the initial development of circular jets. *4th Symp. on Turbulence in Liquids*, pp. 333–342. Science.

BRUUN, H. H. 1977 A time-domain analysis of the large-scale flow structure in a circular jet. Part 1. Moderate Reynolds number. *J. Fluid Mech.* **83**, 641–672.

CORKE, T. & MANGANO, R. 1987 Transition of a boundary layer: controlled fundamental-subharmonic interactions. In *Proc. Symp. on Turbulent Management and Relaminarization, Bangalore, India*, pp. 199–213. Springer.

CORKE, T. & MANGANO, R. 1989 Resonant growth of three dimensional modes in transitioning Blasius boundary layers. *J. Fluid Mech.* **209**, 93–150.

CORKE, T. C., SHAKIB, F. & NAGIB, H. M. 1985 Effects of low amplitude forcing on axisymmetric jet flows. *AIAA Shear Flow Control Conference, Boulder, Colorado, AIAA*-85-0573.

DRUBKA, R. E. 1981 Instability in near field of turbulent jets and their dependence on initial conditions and Reynolds number. Ph.D. thesis, Illinois Institute of Technology.

DRUBKA, R., REISENTHEL, P. & NAGIB, H. 1989 The dynamics of low initial disturbance turbulent jets. *Phys. Fluids* A **1**, 1723–1735.

FFOWCS WILLIAMS, J. E. & KEMPTON, A. J. 1978 The noise from the large-scale structures of a jet. *J. Fluid Mech.* **84**, 673–694.

GUTMARK, E. & HO, C.-M. 1983 Preferred modes and the spreading rates of jets. *Phys. Fluids* **26**, 2932–2938.

HASSELMAN, K., MUNK, W. & MCDONALD, G. 1963 Bispectrum of ocean waves. In *Proc. Symp. on Time Series Analysis* (ed. M. Rosenblatt), pp. 125–139. John Wiley.

HINICH, M. J. & CLAY, C. S. 1968 The application of the discrete Fourier transform in the estimation of power spectra, coherence, and bispectra of geophysical data. *Rev. Geophys.* **6**, 347–363.

HO, C.-M. 1981 Local and global dynamics of free shear layers. In *Proc. Symp. on Numerical and Physical Aspects of Aerodynamic Flows, Long Beach, CA*, pp. 521–533. Springer.

HO, C.-M. & HUANG, L.-S. 1982 Subharmonics and vortex merging in mixing layers. *J. Fluid Mech.* **119**, 443–473.

HO, C.-M. & HUERRE, P. 1984 Perturbed free shear layers. *Ann. Rev. Fluid Mech.* **16**, 365–424.

HUSSAIN, A. K. M. F. & CLARK, A. R. 1981 On the coherent structure of the axisymmetric mixing layer: a flow visualization study. *J. Fluid Mech.* **104**, 263–295.

HUSSAIN, A. K. M. F. & ZAMAN, K. B. M. Q. 1981 The preferred mode of the axisymmetric jet. *J. Fluid Mech.* **110**, 39–71.

KELLY, R. E. 1967 On the resonant interaction of neutral disturbances in inviscid shear flows. *J. Fluid Mech.* **31**, 789–799.

KIBENS, V. 1979 On the role of vortex pairing in jet noise generation. *McDonnel Douglas Research Laboratory Rep.*

KNISELY, C. & ROCKWELL, D. 1981 Self-sustained low-frequency components in an impinging shear layer. *J. Fluid Mech.* **116**, 157–187.

KUSEK, S. M., CORKE, T. C. & REISENTHEL, P. 1990 Seeding of helical modes in the initial region of an axisymmetric jet. *Expts Fluids* (to appear).

LAUFER, J. & ZHANG, J. X. 1983 Unsteady aspects of a low Mach number jet. *Phys. Fluids* **26**, 1740–1750.

LII, K. S., ROSENBLATT, M & VAN ATTA, C. 1976 Bispectral measurements in turbulence, *J. Fluid Mech.* **77**, 45–62.

MATTINGLY, G. E. & CHANG, C. C. 1974 Unstable waves on an axisymmetric jet column. *J. Fluid Mech.* **65**, 541–560.

MICHALKE, A. 1965 On spatially growing disturbance in an inviscid shear layer. *J. Fluid Mech.* **23**, 521–544.

MICHALKE, A. 1971 Instabilitat eines Kompressiblem Ruden Friestrahls unter Berucksichtingung des Einflusses der Strahlgrenzschichtdicke, *Z. Fluzwiss.* **9**, 319–328.

MIKSAD, R., JONES, F. & POWERS, E. 1983 Measurements of nonlinear interactions during natural transition of a symmetric wake. *Phys. Fluids* **26**, 1402–1409.

MIKSAD, R. W., JONES, F. L., POWERS, E. J., KIM, Y. C. & KHADRA, L. 1982 Experiments on the role of amplitude and phase modulations during transition to turbulence. *J. Fluid Mech.* **123**, 1–29.

MONKEWITZ, P. A. 1988 Subharmonic resonance, pairing and shredding in the mixing layer. *J. Fluid Mech.* **188**, 223–252.

PETERSON, R. A. 1978 Influence of wave dispersion on vortex pairing in a jet. *J. Fluid Mech.* **89**, 469–495.

PIERREHUMBERT, R. T. 1980 The structure and stability of large vortices in an inviscid flow. Ph.D. thesis, Massachusetts Institute of Technology.

REISENTHEL, P. & CORKE, T. C. 1983 Application of spectral entropy methods to non-stationary flow problems. *Bull. 36th Am. Phys. Soc. Fluids Division Meeting.*

SAROHIA, V. & MASSIER, P. F. 1978 Experimental results of large-scale structure in jet flows and their relation to jet noise production. *AIAA J.* **16**, 831.

SHAKIB, F. 1985 Evolution and interaction of instability modes in an axisymmetric jet. M.S. thesis, Illinois Institute of Technology.

SOLIS, R., MIKSAD, R. & POWERS, E. 1986 Experiments on the influence of mean flow unsteadiness on the laminar–turbulent transition of a wake. *Proc. Tenth Symp. on Turbulence in Liquids, Rolla, Missouri.* Science.

WILLE, R. 1963 Beitrage Zur Phanomenologie der Freistrahlen. *Z. Flugwiss.* **11**, 222–233.

WINANT, C. D. & BROWAND, F. K. 1974 Vortex pairing: the mechanism of turbulent mixing-layer growth at moderate Reynolds number. *J. Fluid Mech.* **63**, 237–255.